771

3209

R and D CENTER LABORATORY

TECHNICAL REPORT

NO. 12612

INFRARED RADIATION IN A NATURALLY OBSCURED ATMOSPHERE, Propagation of

Contract DAAK30-79-G-0002

JAN 1982

L.W. WINCHESTER, Jr.
GG GIMMESTAD
S.M. LEE
Keweenaw Research Center
Michigan Technological Univ
Houghton, MI

by and DAVID K. WILLBURN

US Army Tank-Automotive Command
ATTN: DRSTA-ZSC
Warren, MI 48090

U.S. ARMY TANK-AUTOMOTIVE COMMAND
RESEARCH AND DEVELOPMENT CENTER
Warren, Michigan 48090

NOTICES

The findings in this report are not to be construed as an official Department of the Army position.

Mention of any trade names or manufacturers in this report shall not be construed as advertising or as an official indorsement or approval of such products or companies by the US Government.

Destroy this report when it is no longer needed. Do not return it to the originator.

SECURITY CLASSIFICATION OF THIS PAGE (When Data Entered)

REPORT DOCUMENTATION PAGE

READ INSTRUCTIONS BEFORE COMPLETING FORM

1. REPORT NUMBER: 12612	2. GOVT ACCESSION NO.
3. RECIPIENT'S CATALOG NUMBER	
4. TITLE (and Subtitle): Propagation of Infrared Radiation In A Naturally Obscured Atmosphere	5. TYPE OF REPORT & PERIOD COVERED: FINAL REPORT 13 Feb 1980 - 31 Dec 1980
	6. PERFORMING ORG. REPORT NUMBER
7. AUTHOR(s): L.W. Winchester, Jr. G.G. Gimmestad S.M. Lee and D.K. Wilburn	8. CONTRACT OR GRANT NUMBER(s): DAAK30-79-G-0002 Delivery Order 0007
9. PERFORMING ORGANIZATION NAME AND ADDRESS: Keweenaw Research Center Michigan Technological University Houghton, MI 49931	10. PROGRAM ELEMENT, PROJECT, TASK AREA & WORK UNIT NUMBERS
11. CONTROLLING OFFICE NAME AND ADDRESS: U.S. Army Tank-Automotive Command Warren, MI 48090	12. REPORT DATE: July 1981 13. NUMBER OF PAGES: 55
14. MONITORING AGENCY NAME & ADDRESS (if different from Controlling Office)	15. SECURITY CLASS. (of this report): Unclassified 15a. DECLASSIFICATION/DOWNGRADING SCHEDULE: N/A

16. DISTRIBUTION STATEMENT (of this Report)

Distribution Unlimited

17. DISTRIBUTION STATEMENT (of the abstract entered in Block 20, if different from Report)

18. SUPPLEMENTARY NOTES

19. KEY WORDS (Continue on reverse side if necessary and identify by block number)

atmospheric transmission
infrared transmission
obscured atmospheres
infrared extinction
visible extinction

20. ABSTRACT (Continue on reverse side if necessary and identify by block number)

An integrated model of target vehicle signatures must include a description of the effect of transmission of electromagnetic radiation through the atmosphere between the target and the threat sensor devices. A number of models published by various investigators are in use to describe this transmission phenomenon. These models predict fairly accurately the attenuation of light as it propagates through clear air, indicating that they account for the molecular absorption reasonably well. They are not as

DD FORM 1 JAN 73 1473 EDITION OF 1 NOV 65 IS OBSOLETE

SECURITY CLASSIFICATION OF THIS PAGE (When Data Entered)

accurate when the atmosphere contains small particles such as those in rain, fog, snow, etc. In adverse atmospheric conditions, the scattering process becomes comparatively more important and must also be considered.

In this report, a detailed investigation is presented for the scattering of infrared radiation by atmospheric aerosols. The theoretical analysis is compared to the measured data obtained at the Keweenaw Research Center (KRC). The analysis and the results are compared to the prediction of other available models. In addition, the implication of the present work on the ongoing TACOM/KRC modeling effort of target signature is discussed.

TABLE OF CONTENTS

LIST OF TABLES

LIST OF FIGURES

PREFACE

The work described in this technical report is sponsored by the Countermeasure Function, DRSTA-ZSC of the U.S. Army Tank Automotive Command under contract DAAK 30-79-G-0002, D.O. 0007. The Atmospheric Transmission facility at the Keweenaw Research Center is operated in support of the Vehicle Signature Modeling effort and is dedicated to a study of the transmission properties of the atmosphere through snow and rain. For further information contact the Keweenaw Research Center, R.R. 1, Box 94-D, Calumet, Michigan 49913 or the Tank Automotive Command, DRSTA-ZSC, Warren, Michigan 48090.

1. INTRODUCTION

Attenuation of electromagnetic radiation in the atmosphere is due to absorption and scattering by the constituents of the atmosphere. Absorption by air molecules such as N_2, O_2, O_3, CH_4, and CO has been modeled by many authors too numerous to list. An atlas of all absorption lines of the major atmospheric gases compiled by McClatchey, et al. (1973) put all the available results in one summarized form, which is often used as a representative reference. The parameters include the frequency, half width and oscillator strength of the resonance and the energy and relevant quantum numbers of the lower state. Using this compilation, it is possible to calculate absorption by a clear (non-particulate) atmosphere at wavelengths greater than 1.0 micrometer. Such a calculation is very useful when dealing with a very narrow spectral region (a laser line) but time consuming for a broad band. A low resolution transmission program (LOWTRAN) has been developed by Selby, et al. (1978) and has proved to be an accurate predictor of atmospheric absorption in clear air. Smith, et al. (1978) developed a fast high resolution atmospheric transmission program (FASCODE) with the capability of using Doppler, Lorentz, and/or Voight line profiles. Such a program is valuable for the investigation of light transmission in a layered atmosphere where the line broadening process varies with altitude (pressure). This study is concerned with the atmospheric boundary layer and therefore, the values of the pressure and density of each constituent gas are assumed constant along the path.

Molecules of gases present in the atmosphere are small compared to the wavelengths of radiation of interest in this study (0.4 to 14.0 micrometers) and any scattering of radiation of these molecules is described by Rayleigh scattering (Fabelinskii, 1968; Shifrin, 1968). The most important features of this process are the λ^{-4} dependence of the scattered intensity and the Rayleigh phase function

$$f_R(\Theta) = \frac{3}{4} (1 + \cos^2\Theta) \qquad (1)$$

where Θ is the scattering angle. Molecular scattering is a negligible effect on the short ray paths (one kilometer) considered here.

Several studies of extinction of electromagnetic radiation by fog, rain, and snow which have appeared in the literature have often presented conflicting results. Chu and Hogg (1960) measured the extinction of radiation at wavelengths of 0.63, 3.5, and 10.6 micrometers in fog, rain, and snow. They obtained a loss of 15.5 I + 2.66 dB/km at 0.6328 micrometer in rain where I is rainfall rate. The loss rate was obtained by a least - square fit to data between 12.5 and 100 millimeter/hour rainfall. They calculated a single scattering correction term using van de Hulst's (1957) approximation of the extinction efficiency and by assuming a Gaussian pattern to the forward scattering beam. The agreement between measurement and calculation was within 10% for 0.6328 micrometer radiation.

Sokolov and Sukhonin (1971) examined the effect of the form of the drop distribution on calculations of extinction by rain. They compared the measurements of Chu and Hogg (1960) with computations using the drop size distributions of Laws and Parsons (1943), Best (1950), and Barteneva, et al. (1967) for rains of intensity between 0 and 100 mm/hr. As Sokolov and Sukhonin did not consider the possibility of any scattered light reaching the receiver, the extinctions of 0.63, 3.5, and 10.6 micrometers are all identical as shown in Figure 1. The data of Chu and Hogg had also been plotted for the purposes of comparing theory and experiment. Sokolov and Sukhonin concluded that the distribution due to Barteneva, et al. (1967) gave the best agreement with experiment. A ray tracing method was used to calculate the backscatter amplitude function. Bisyarin, et al. (1971) measured the attenuation coefficient of 0.63 and 10.6 micrometer radiation in snow and rain over a 1.36 km path. In snow they found the following relations

$$\beta_{0.63} = 10.8\ I^{0.53} \tag{2}$$

$$\beta_{10.6} = 15.1\ I^{0.71} \tag{3}$$

where I is the snowfall rate measured in millimeters per hour. Rain measurements were made for rainfall intensities of less than 10 millimeters per hour and are inconclusive.

Recent data from the OPAQUE measurement program at the German station at Birkhof (Jessen, et al., 1980) have indicated that the drop size distribution of rain is an important factor in computing transmission. The

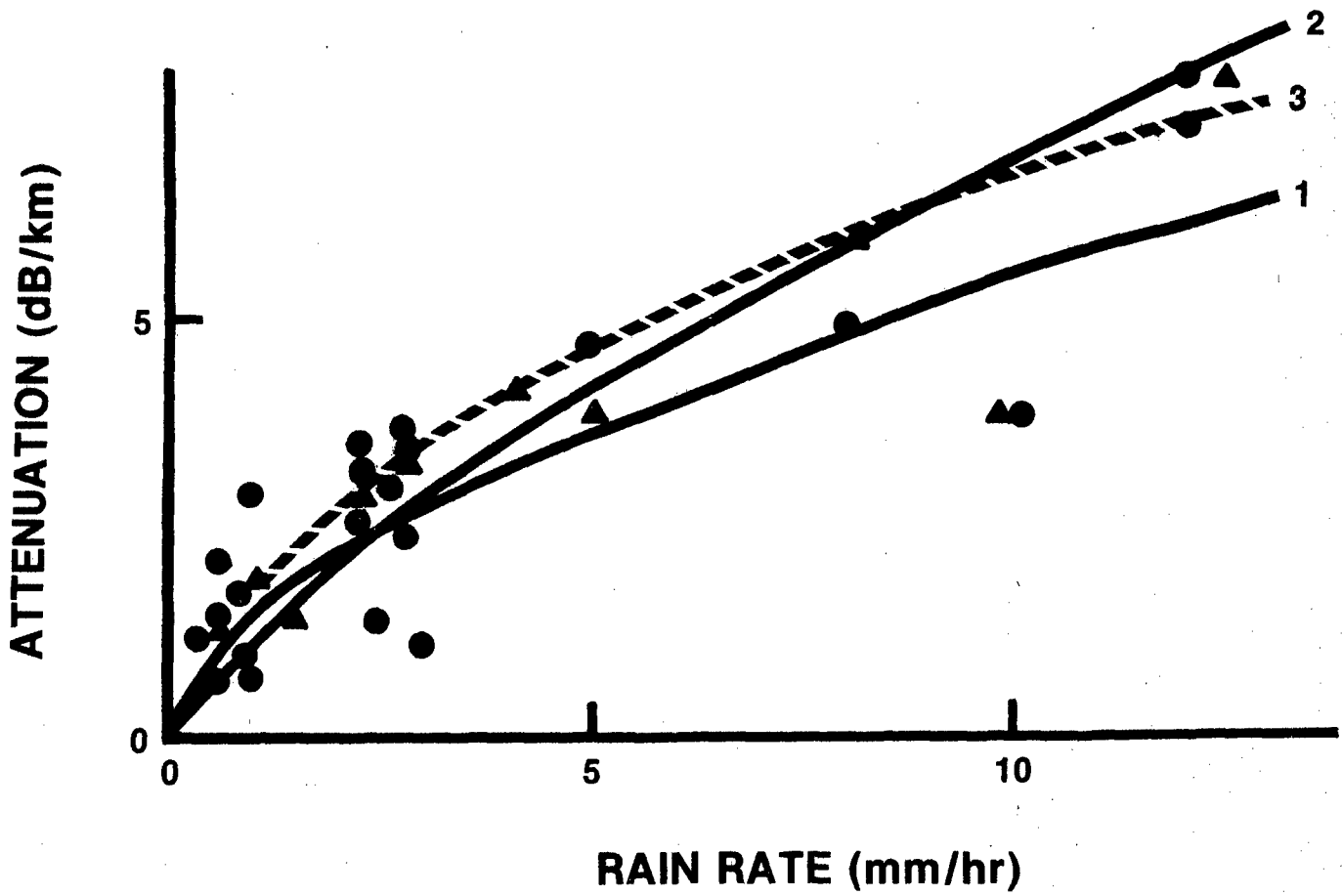

Fig. 1. Comparison of attenuations versus rain intensity for several drop size distributions (taken from Sokolov and Sukhonin, 1970). Curves 1 and 2 use the distributions of Best (1950) and Barteneva, et al (1967) while curve 3 is a least squares fit.

authors also place importance on the knowledge of aerosol physics and humidity in order to understand transmission through the atmosphere. The particles which have the largest effect on scattering/absorption are those comparable in size to the wavelength of the radiation. The small rain droplets, comparable in size to some fog droplets, do not have the intense diffraction peak present in scattering by large particles. When dealing with any scattering medium, knowledge of the particle size distribution is of prime importance in understanding the scattering process.

The meteorological visibility is a required input to the current level of military models such as GAP (Moulton, et al., 1976) and E-O SAEL (Duncan, et al., 1979) which predict the attenuation in various infrared regions of the spectrum in adverse weather conditions. Using Kochsmeider's relation, the extinction coefficient at 0.55 micrometer is given by

$$\beta_{0.55} = \frac{3.912}{V} \tag{4}$$

where V is the meteorological visibility. The visible extinction coefficient is then used to calculate the extinction coefficient in the desired infrared band by assuming that the logarithm of the infrared extinction coefficient is either a linear (Moulton, et al., 1976; Duncan, et al., 1979) or quadratic (Shields, 1978) function of the logarithm of the extinction coefficient at 0.55 micrometer. Experimental data collected at Fort A.P. Hill, Virginia, and at Grafenwoehr, Germany, were used to obtain the necessary coefficients of the above mentioned functions for such general types of weather conditions as fog, rain, and snow. Fog was further broken down into three categories: "dry", "wet", and "all". A fog was classified "wet" if condensation collected on exposed metal surfaces and "dry" otherwise. The major weakness of this approach is that the extinction coefficient in the visible region of the spectrum is not calculated from the weather parameters. The results for attenuation of radiation in the 3 to 5 micrometer region compared to attenuation at 0.55 micrometer by "all", "dry", and "wet" fogs are shown in Figures 2, 3, and 4, respectively, which were taken from the report by Turner, et al. (1980). The visibility ranges from 0.4 to 2.5 kilometers. Turner, et al. (1980) note that the variance in the data is much less for "dry" fogs than for "wet" fogs, and suggests that the atmospheric conditions vary less for "dry" fogs as far as the intrinsic particle properties are concerned. A similar result

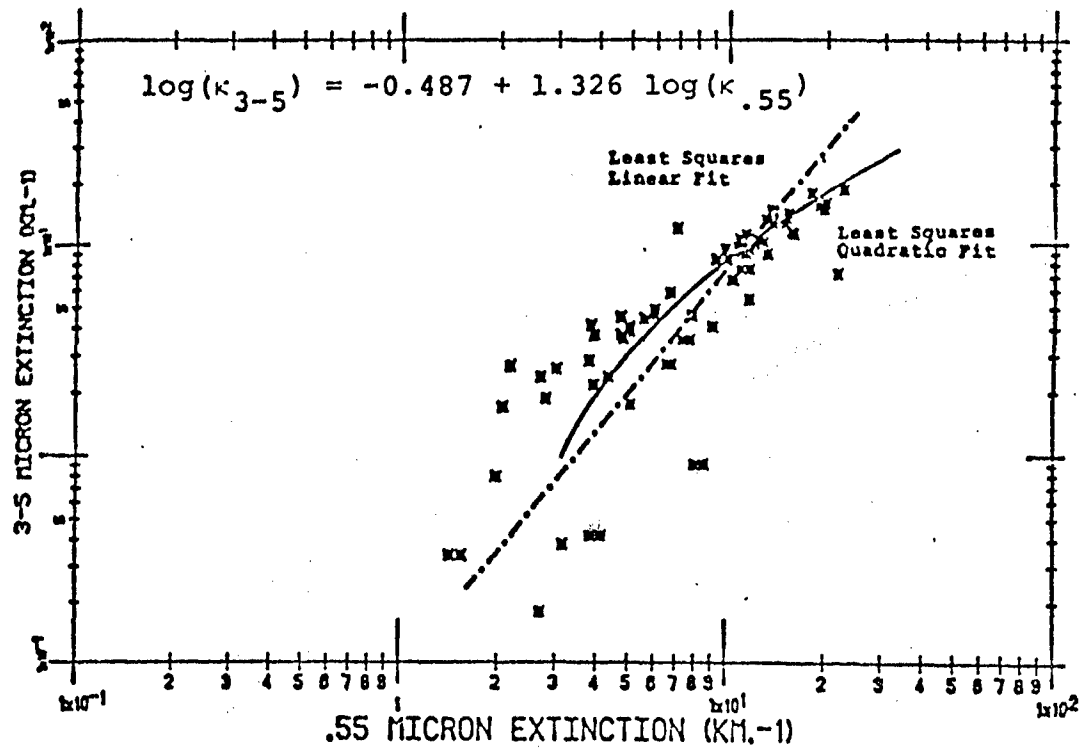

Fig. 2. Volume Extinction coefficients in the 3 to 5 micrometer band and at 0.55 micrometers for "all" fogs. (A.P. Hill data between April, 1977 and November, 1977, taken from Turner, et.al. (1980))

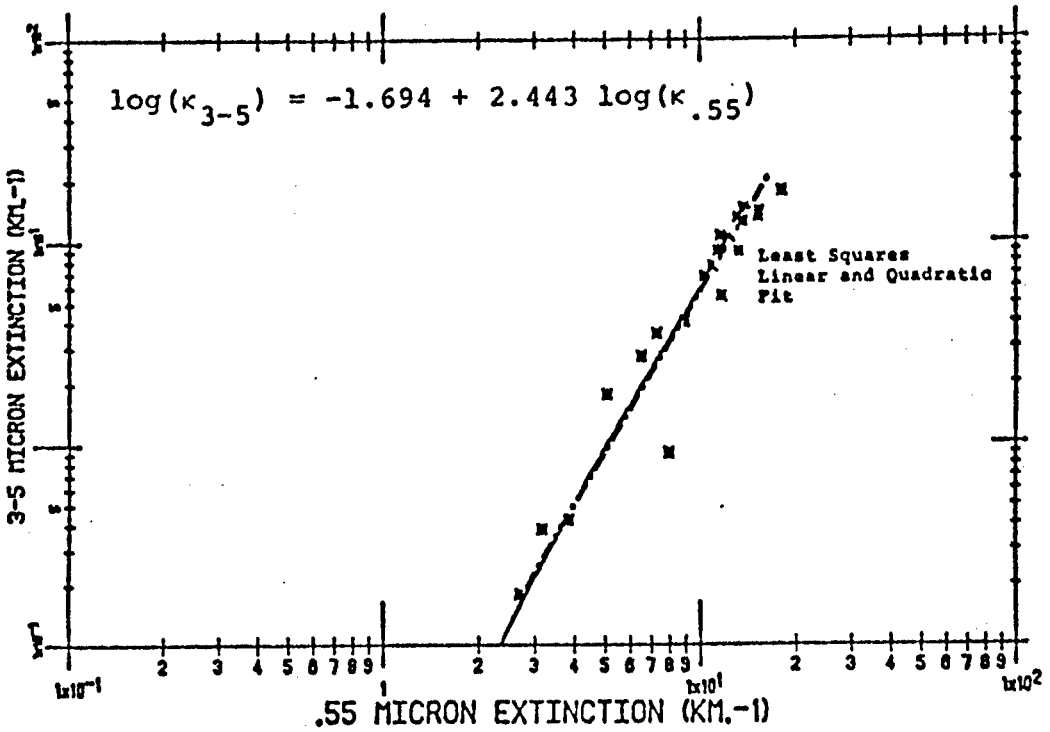

Fig. 3. Volume extinction coefficients in the 3 to 5 micrometer band and at 0.55 micrometers for "dry" fogs. (A.P. Hill data between June, 1977 and November, 1977, taken from Turner, et.al. (1980))

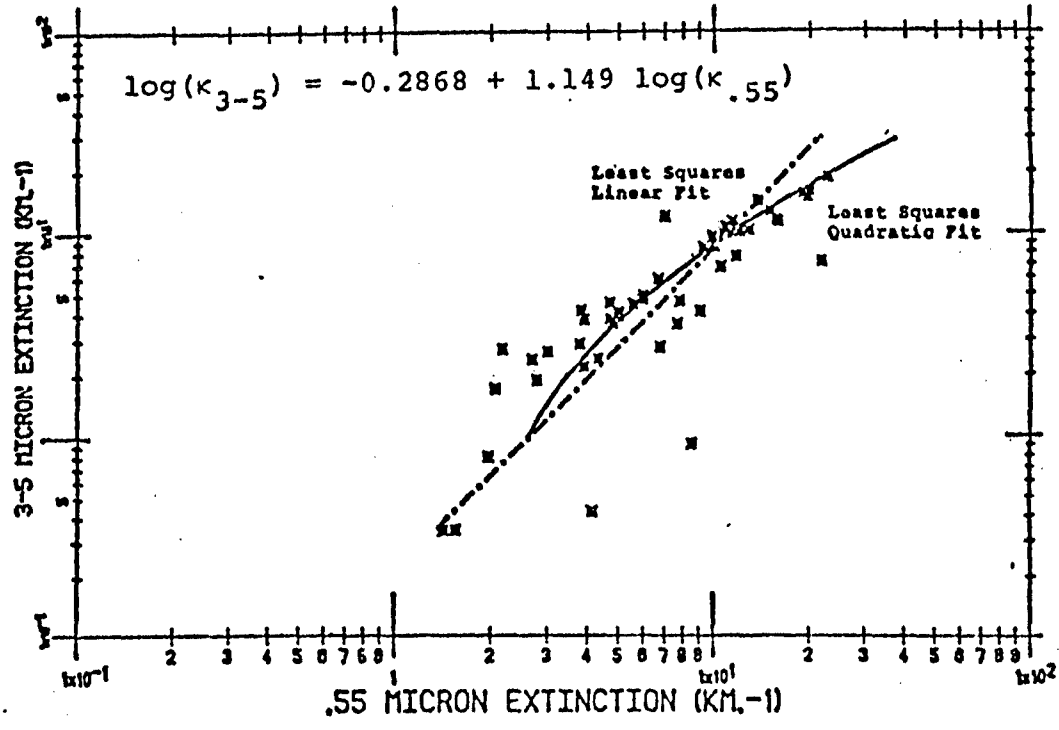

Fig. 4. Volume Extinction coefficient in the 3 to 5 micrometer band and at 0.55 micrometers for "wet" fogs. (A.P. Hill data between April, 1977 and November, 1977, taken from Turner, et.al. (1980))

was obtained for extinction in the 8 to 12 micrometer region as shown in Figures 5, 6, and 7. Measurements made for a single day are in much better agreement with a linear equation, as shown by some typical data in Figure 8. The data from Grafenwoehr and Fort A.P. Hill were collected at thirty minute intervals. As the time between measurements is long compared with fog lifetimes, it is not possible for the GAP model to follow the evolution of fogs as they form and dissipate.

The GAP model considers the molecular state of the air as part of the fog, in that it does not separate extinction into air and fog droplet contributions. Absorption by air molecules, particularly in the infrared region, is a function of temperature, pressure, and the density of water in the vapor phase (not to be confused with the water content of the fog). Absorption by air molecules can and should be computed separately from extinction by the fog.

Winchester, et al. (1980a) have shown that the contribution of scattering processes to extinction is comparable to that of absorption in the infrared and dominates extinction in the visible range. The model for extinction of radiation in fogs must include an algorithm for calculating the ability of the detection or viewing device to collect scattered radiation (Bruscaglioni, 1978 and 1979; Buscaglioni and Ismaelli, 1978 and 1979; Winchester, et al. (1980 a and b). Such a feature will allow for implementation of the model for any set of equipment, not just the apparatus on which the original data were taken, as in the case of the GAP model.

The large scatter in the GAP and OPAQUE data results from combining data from many different fogs into one data plot. Because fogs are characterized by the particle size distribution function, and because the ratio of the infrared extinction to the visible extinction is very sensitive to particle size, a large scatter in fog extinction data should be expected when considering many fogs. Another contribution to extinction is absorption by the air. This contribution is dependent on weather parameters such as temperature and pressure and must be predicted separately in order to isolate the extinction due to fog. As Turner, et al (1980) have suggested, the linear relation between the logarithms of the extinction coefficients may be a good approximation for one fog. If measurements are made at intervals on the order of a minute instead of

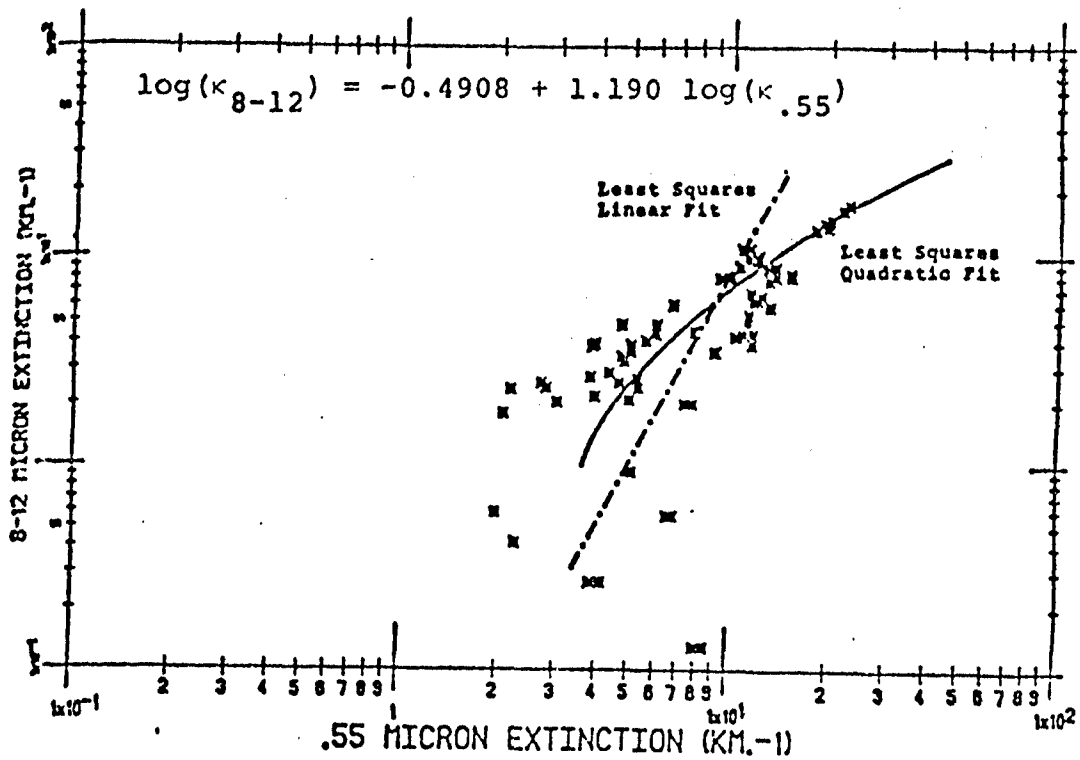

Fig. 5. Volume extinction coefficient in the 8 to 12 micrometer band and at 0.55 micrometers for "all" fogs. (A.P. Hill data between April, 1977 and November, 1977, taken from Turner, et.al. (1980))

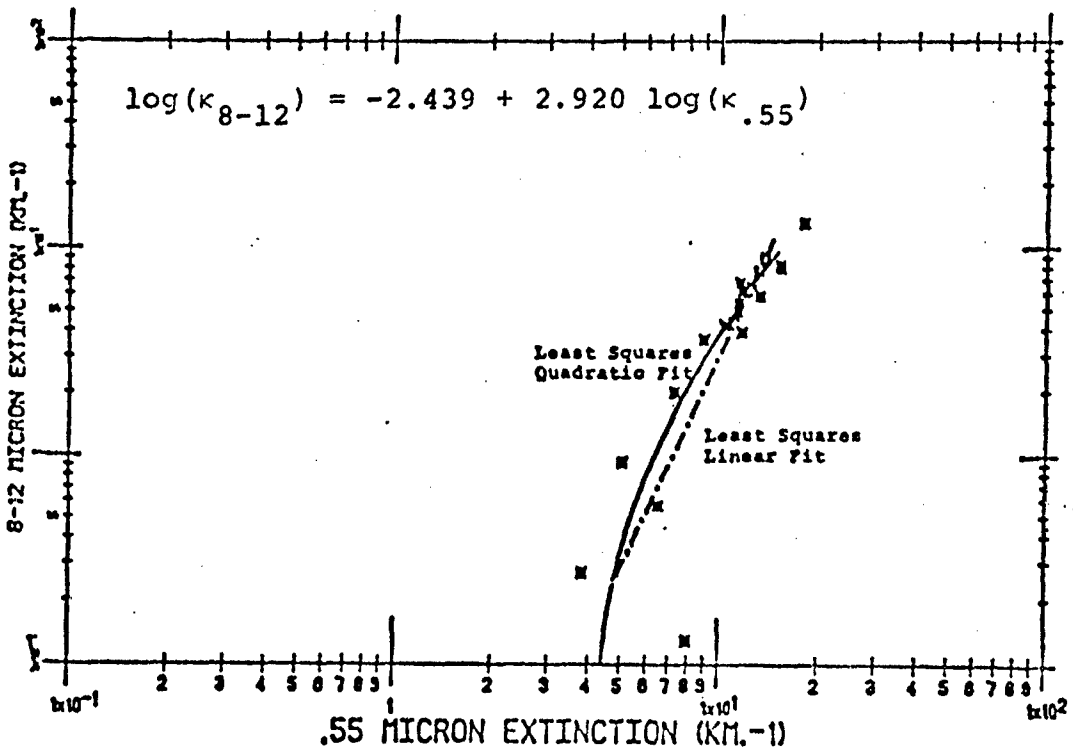

Fig. 6. Volume extinction coefficient in the 8 to 12 micrometer band and at 0.55 micrometers for "dry" fogs. (A.P. Hill data between June, 1977 and November, 1977, taken from Turner, et.al. (1980))

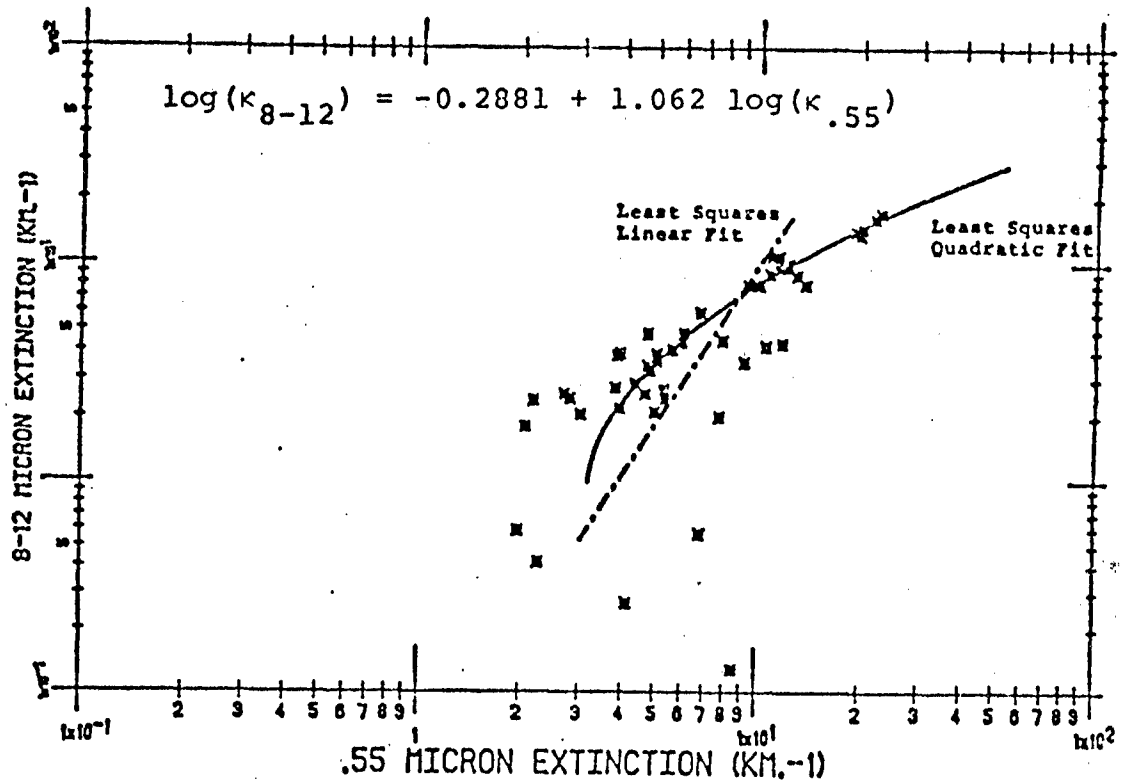

Fig. 7. Volume extinction coefficient in the 8 to 12 micrometer band and at 0.55 micrometer for "wet" fogs. (A.P. Hill data between April, 1977 and November, 1977, taken from Turner, et.al. (1980))

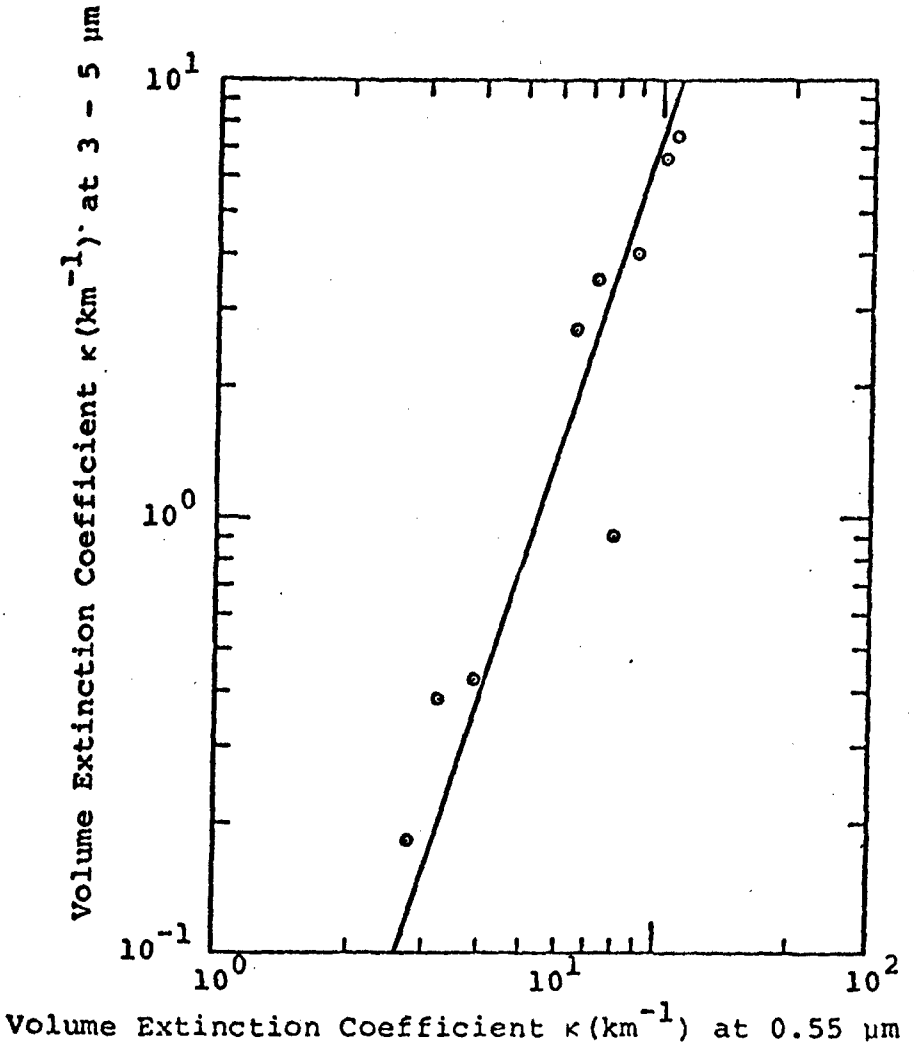

Fig. 8. Variation of the volume extinction coefficient for the 8 to 12 micrometer band and at 0.55 micrometers for "dry" fog data on 16 June 1977. (Taken from Turner, et.al. (1980))

at half-hourly intervals, as in the case of the GAP and OPAQUE data, the extinction of radiation may be studied as the fog evolves. This is clearly evident from data sampled at one minute intervals at the Keweenaw Research Center (KRC), which will be discussed below.

Ideally, both the visible and the infrared extinction coefficients should be calculated separately from a model based on a desired set of weather parameters such as temperature, humidity, particle size distribution function, etc. As shown by Figures 2 through 7, the experimental data from many fogs are too scattered to be described by one line (β_{IR} ranges over one decade at many values of β_{VIS}). However, data taken over the life cycle of one fog, a period of a few hours, indicate that a linear relation between $\ln \beta_{VIS}$ and $\ln \beta_{IR}$ is a good fit. The intercept and slope of the line should be obtainable from a model using the weather parameters mentioned above as inputs.

2. OBJECTIVES

The objectives of the work reported here were to develop improved understanding of, and better models for, the propagation of infrared radiation in an atmosphere containing natural obscurants such as fog, rain, and snow. The approach taken consisted of reviewing previous work, performing actual measurements of extinction in obscured atmospheres, and a good deal of calculation and modeling.

3. SUMMARY

A model of the effects of countermeasures to ground vehicle infrared signatures on threat weapon system performance must take into account the propagation of infrared radiation through the earth's atmosphere. A number of models for atmospheric transmission have been published by various authors, and one of them (LOWTRAN) works well for clear air, indicating that it accounts for molecular absorption reasonably well. When particles are present in the atmosphere, existing models are not as good. The GAP model (Moulton, et al., 1976) addresses this problem by relating infrared extinction to visible extinction (found from visibility). The GAP model has been found to have the following weaknesses:

(1) It makes no distinction between molecular absorption and extinction by particles;

(2) Infrared extinction is calculated from visibility, rather than from weather parameters;

(3) GAP model parameters are obtained by fitting curves to experimental data which may be instrument-dependent;

(4) In fog, the model predictions are representative only of specific fogs in certain locations.

The phase function has been found to be of great importance in determining the transmission of radiation through a scattering atmosphere. The computation of transmission through a standard rain using different phase functions illustrates that the phase function which corresponds to particle size distribution of particles whose sizes differ greatly cannot be easily approximated by an analytical function such as the Henyey-Greenstein (1941) and Kagiwada-Kalaba (1967) phase functions. The added dimension of finite size receivers increases the need for knowledge of the scatterers and hence the phase function when applying relations derived from data obtained on one set of appartus to another instrument.

A detailed investigation is presented for the scattering of infrared radiation by the atmospheric aerosols. The theoretical analysis is compared to the measured data obtained at the Keweenaw Research Center. The analysis and the results are compared to the prediction of other available models. In addition, the implication of the present work to the on-going TACOM modeling effort of target signatures is discussed.

4. RECOMMENDATIONS

For calculating infrared absorption due to molecules, LOWTRAN should be used.

In the presence of naturally occurring particles, a new model is needed which will calculate infrared extinctions from weather parameters. A beginning of such a model has been made as a part of this study, the calculation of infrared transmission versus rain rate (discussed later); this model needs to be validated.

While models of the GAP type have been shown to be instrument-dependent, a linear relation does exist between the visible and infrared

extinction coefficients for a given pair of instruments. A model of the GAP type should be used as the atmospheric transmission model in fog, rain, and snow until a scattering model is fully developed.

An approach to an improved model for infrared extinction in fog is suggested by measurements at KRC, and this model can be actively pursued by augmenting the weather station to include a fog drop size measuring instrument.

A model of snow extinction versus snowfall rate can be attempted by adding to the weather station instrumentation to measure snowfall rate.

Laser designators and rangefinders operate at 1.06 and 10.6 micrometers; installation of lasers at these wavelengths on the transmission range is desirable.

5. THEORETICAL FORMULATION

Extinction by particulate matter is in general due to both scattering and absorption. In order to assess the relative importance of scattering versus absorption, the complex index of refraction must be known. Scattering is governed by the real part of the index of refraction while absorption is a function of the imaginary part. The phase function $f(\Theta, \phi)$, namely the angular dependence of the scattered light, is usually normalized

$$\tilde{\omega} = \frac{1}{4\pi} \int_{4\pi} f(\Theta, \phi)\, d\Omega \tag{5}$$

where $\tilde{\omega}$ is the albedo, or ratio of scattering to total extinction (absorption plus scattering) and Θ and ϕ are angles describing the scattering direction in spherical polar coordinates. In practice, scattering is assumed to be independent of the azimuthal angle ϕ so Eq. 5 may be rewritten

$$\tilde{\omega} = \frac{1}{2} \int_{o}^{\pi} f(\Theta) \sin\Theta \; d\Theta \tag{6}$$

where Θ is the scattering angle. As the scattering parameter $\chi = 2\pi\, r/\lambda$ (where r is the particle radius and λ is the wavelength of the incident electromagnetic radiation) is increased, the amount of forward scattering (near 0°) increases, while back scattering (180°) oscillates, as illustrated in Figure 9 for the case of raindrops illuminated by radiation

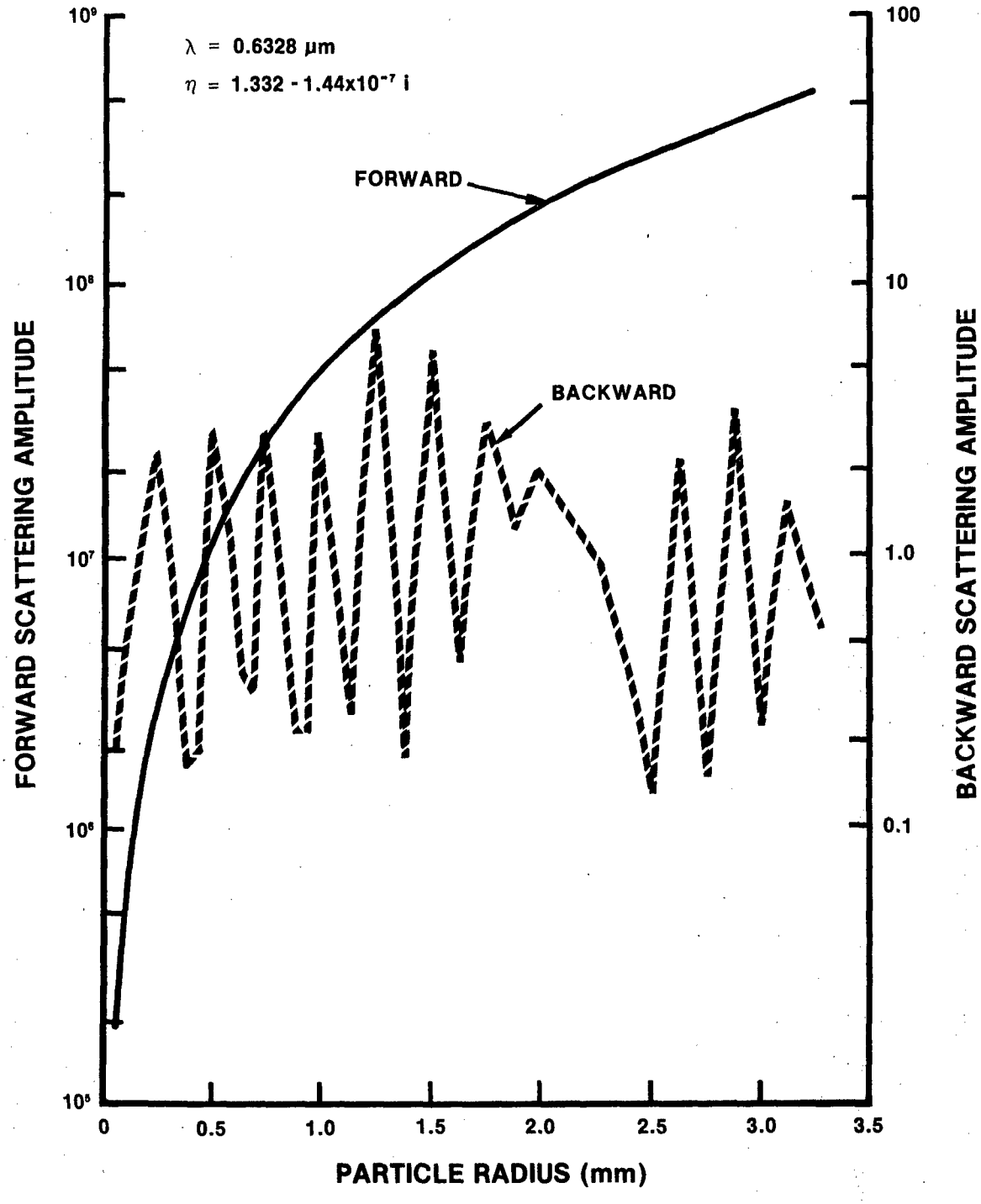

Fig. 9. Variation of the forward and backward scattering intensities with the particle radius

with a wavelength of 0.6328 micrometer from a Helium-Neon laser. When calculating transmission through a scattering atmosphere, an estimate of the amount of radiation which reaches the detector after experiencing one or more scattering events must be evaluated to determine what order scattering processes are important. Because it is a measure of the angular spread of the scattered radiation, the phase function is essential to an accurate estimate of transmission in a scattering atmosphere.

When calculating the received power of a laser transmissometer the relative importance of both scattering and absorption must be carefully considered. Since some of the scattered radiation will reach the detector after one or more scattering events, the receiver parameters must be considered when evaluating the scattering contribution. The instrument dependence must be accounted for when either measuring or using experimental values of atmospheric extinction under adverse weather conditions such as fog, rain, or snow. The amount of scattering is dependent on the real part of the index of refraction while absorption is related to the imaginary part. For a particle described by a large scattering parameter ($\chi >> 1$), a very strong forward scattering is observed. The shape of the particles is also a factor in determining the phase function. Computations similar to those of Mie (1908) for spheres have been made for cylinders (Kerker, 1969) and regular hexagonal plates (Jacobowitz, 1971).

The geometry of a laser transmissometer is shown in Figure 10. A laser with power I_L and negligible beam divergence is located a distance R from a receiver described by a collection optics diameter H and an acceptance angle α_R.

The amount of power reaching the receiver without undergoing a scattering event is given by

$$I_o = I_L \, g \, P_{NS}(R) \tag{7}$$

where g is a geometrical factor related to the divergence and profile of the laser beam and type and size of the receiver optics. The probability of a photon traveling a distance R without being scattered or absorbed, $P_{NS}(R)$, can be written

$$P_{NS}(R) = \exp\{-[N(\sigma_s + \sigma_A) + \beta_{AIR}]R\} \tag{8}$$

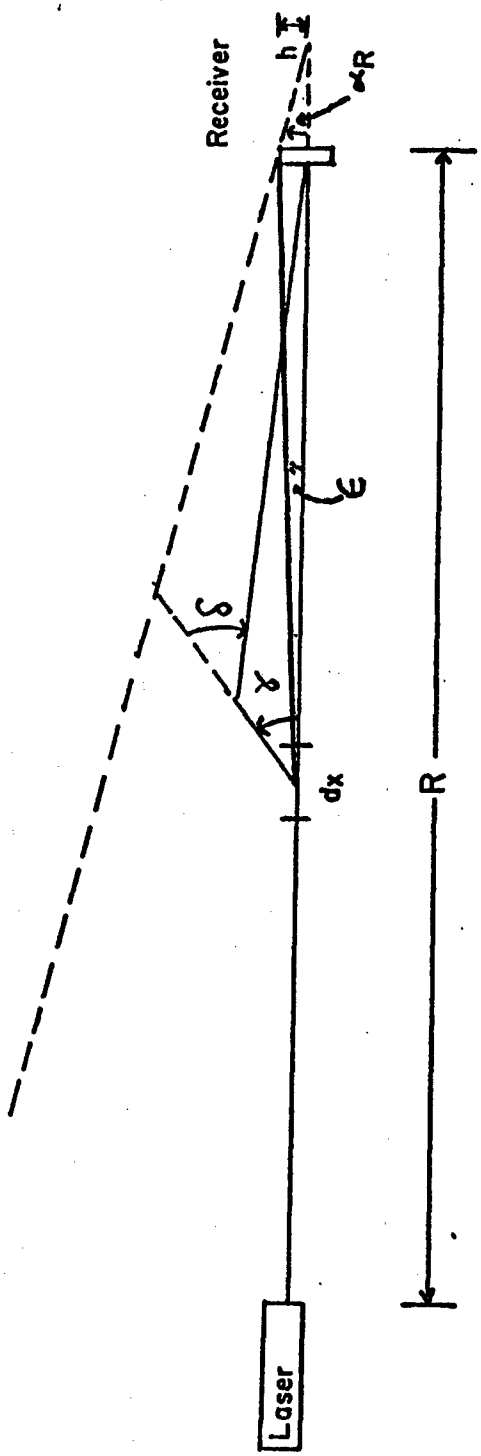

Fig. 10. Laser transmissometer geometry.

where N, σ_s, and σ_A are the number density, scattering cross section and absorption cross section, respectively, of the particles and β_{AIR} is the atmospheric extinction coefficient. The contribution of first order scattering to received power can be written

$$I_1 = I_L \int_o^R \int_{\Omega(\varepsilon)} P_s(x)\, f(\varepsilon)\, P_{NS}\,(R - x)\, d\Omega(\varepsilon)\, dx \tag{9}$$

The probability of scattering in the element dx after traveling a distance x is $P_s(x)\, dx$ where

$$P_s(x) = N\sigma_S\, P_{NS}\,(x) \tag{10}$$

and the phase function $f(\varepsilon)$ has been evaluated at the scattering angle ε. The solid angle $\Omega(\varepsilon)$ is limited by the size of the receiver. The expression for second order scattering is written as

$$I_2 = I_L \int_o^R \int_x^R \int_{\Omega(\gamma)} \int_{\Omega(\delta)} P_s\,(x)\, f(\gamma)\, P_S\,(x' - x)\, f(\delta)\, P_{NS}\,(R - x') \, d\Omega(\delta) d\Omega(\gamma)\, dx'\, dx \tag{11}$$

where the first and second scattering angles are given by γ and δ, respectively.

As can be seen from Eqs. (9) and (11), the magnitude of the scattering contributions to received power depends on the choice of phase function. A critical factor in evaluating the type of scattering is the size parameter χ. When $\chi << 1$ and $|m|\,\chi < 1$, scattering is described by the Rayleigh phase function (Eq. (1)). When dealing with particles where $\chi > 0.1$, a rigorous calculation is required to obtain the phase function. For distributions of spherical or nearly spherical particles, the scattering amplitudes must be calculated for each particle size using Mie theory and averaged over the entire particle size distribution. An analytic phase function developed by Henyey and Greenstein (1941) has been used extensively

$$f_{HG}\,(\Theta) = \frac{(1 - A^2)}{(1 + A^2 - 2A\cos\Theta)^{3/2}} \tag{12}$$

where A is the averaged value of $\cos\Theta$. This phase function has been applied successfully to problems involving radiative transfer and atmospheric distortion of star light. A phase function introduced by Kagiwada and Kalaba (1967) used the ratio of light scattered at 0° to that scattered

at 180° as the single parameter s in the expression

$$f_{KK}(\Theta) = \frac{2}{\ln[s]\left(\frac{s+1}{s-1} - \cos\Theta\right)} \qquad (13)$$

Jacobowitz (1971) has calculated the phase function for hexagonal platelets using ray tracing. His results are reproduced in Figure 11. It is also possible to measure experimentally the phase function of small particles (Huffman and Thursby, 1969; Winchester, et al., 1981). Since it is impossible to separate scattered radiation from unscattered radiation, the forward scattering peak cannot be measured and must therefore be estimated.

In a following section, the formulation outlined above is applied to calculate the effect of a 50.8 mm/hour rain on the KRC laser transmissometer, assuming several different phase functions, and the effect of receiver size on received power is also calculated.

6. EXPERIMENTAL FACILITY

A sheltered outdoor transmission range has been established at KRC, along with facilities to monitor appropriate weather parameters. The range incorporates a folded path, in which radiation goes from the outdoor source out a window to a plane mirror at 500 meters, and is reflected back to the receiver, which is located indoors near the source. The optical arrangement is shown schematically in Figure 12. The advantage of this arrangement , as compared to a straight path, is that all the electronics are at one end, making calibration, maintenance, and temperature control relatively easy.

Visible transmission is measured by using a Helium-Neon laser as a source. The laser emits 0.6 mW CW, is mechanically chopped at 900 Hz, and is aimed at the mirror with no collimating optics. The receiver for the laser is based on cassegrain optics 20 cm in diameter with an 11 milliradian angle of acceptance. The detector is silicon and it is fitted with a narrow-band filter centered at the laser wavelength, 0.6328 micrometer. The detector output is fed into a phase-sensitive amplifier, along with a chopper reference signal. The laser and chopper are shown in Figure 13, and the receiver optics are shown in Figure 14.

The apparatus used for the infrared measurements is the Barnes

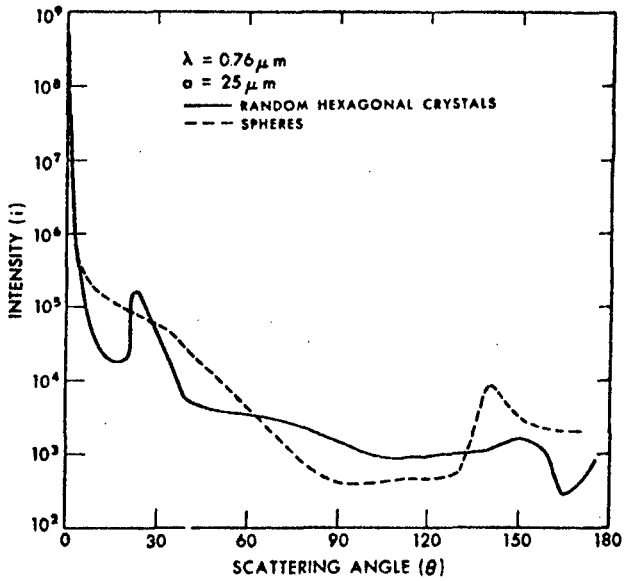

Total intensity, i, for randomly oriented hexagonal prisms compared with that for spheres versus the scattering angle θ.

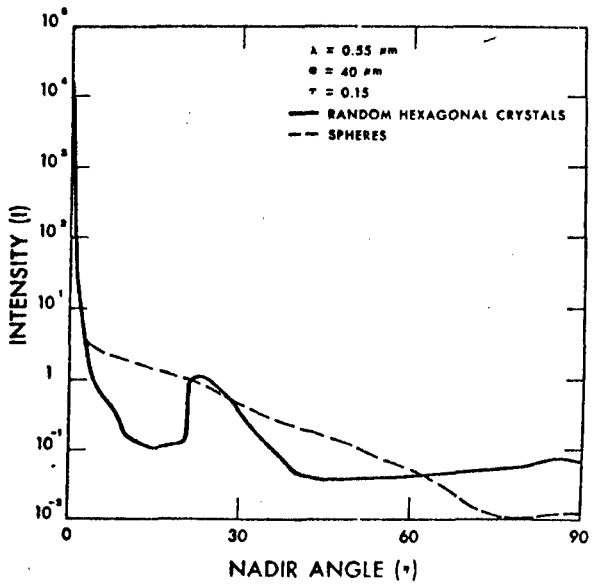

Intensity of radiation transmitted through a model cirrus cloud for a unit incident flux normal to the cloud versus the nadir angle η.

Fig. 11. Phase functions of hexagonal ice crystals calculated using geometrical optics (Jacobowitz, 1971).

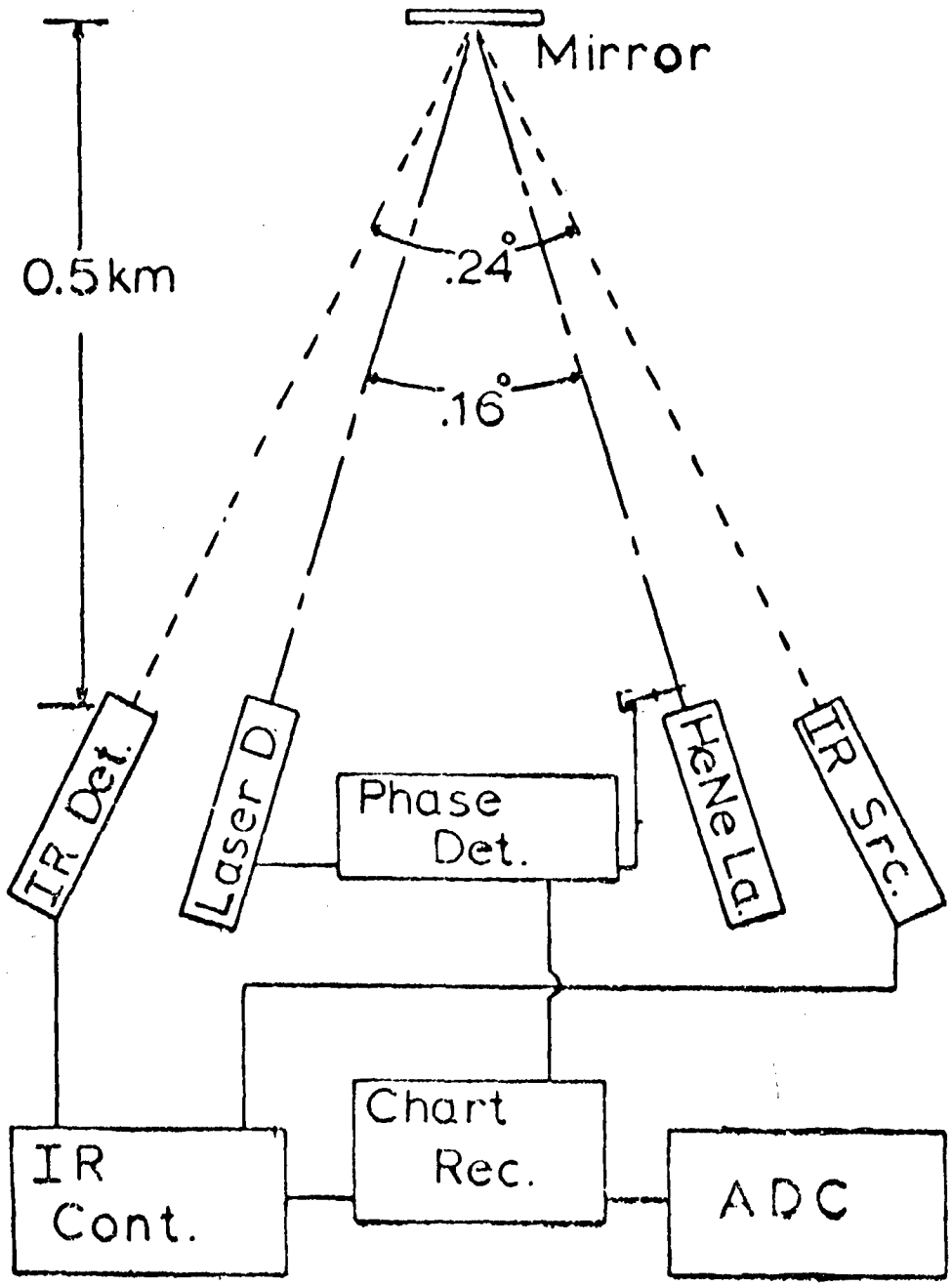

Fig. 12. Schematic diagram of KRC atmospheric transmission range.

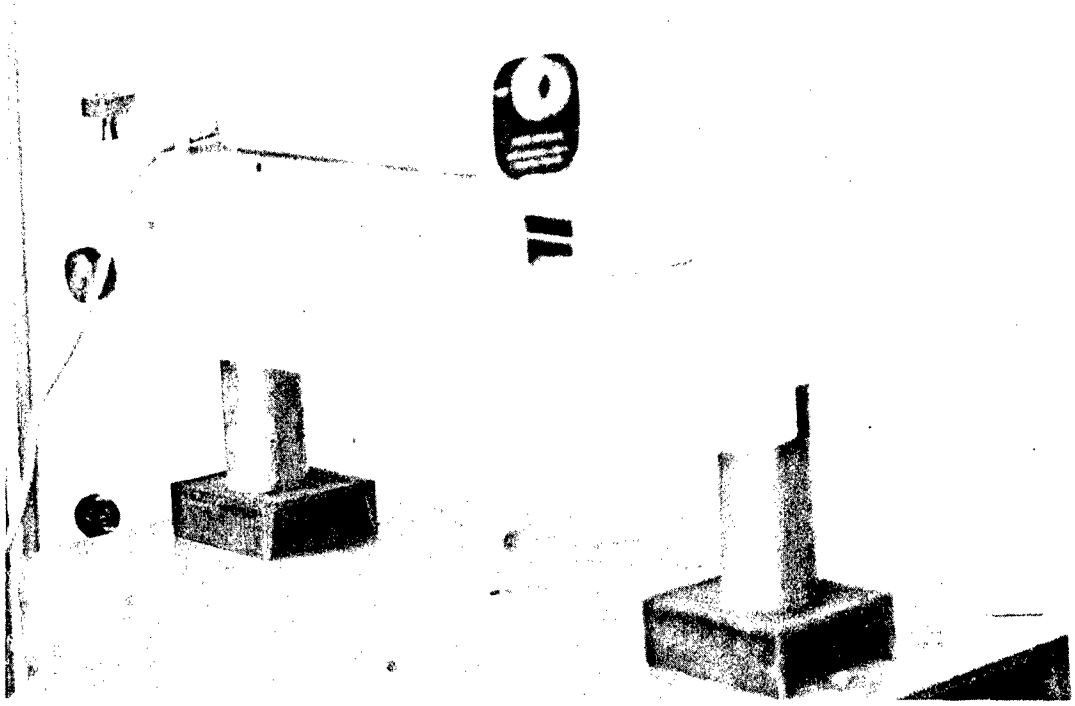

Fig. 13. Helium-Neon Laser and Chopper

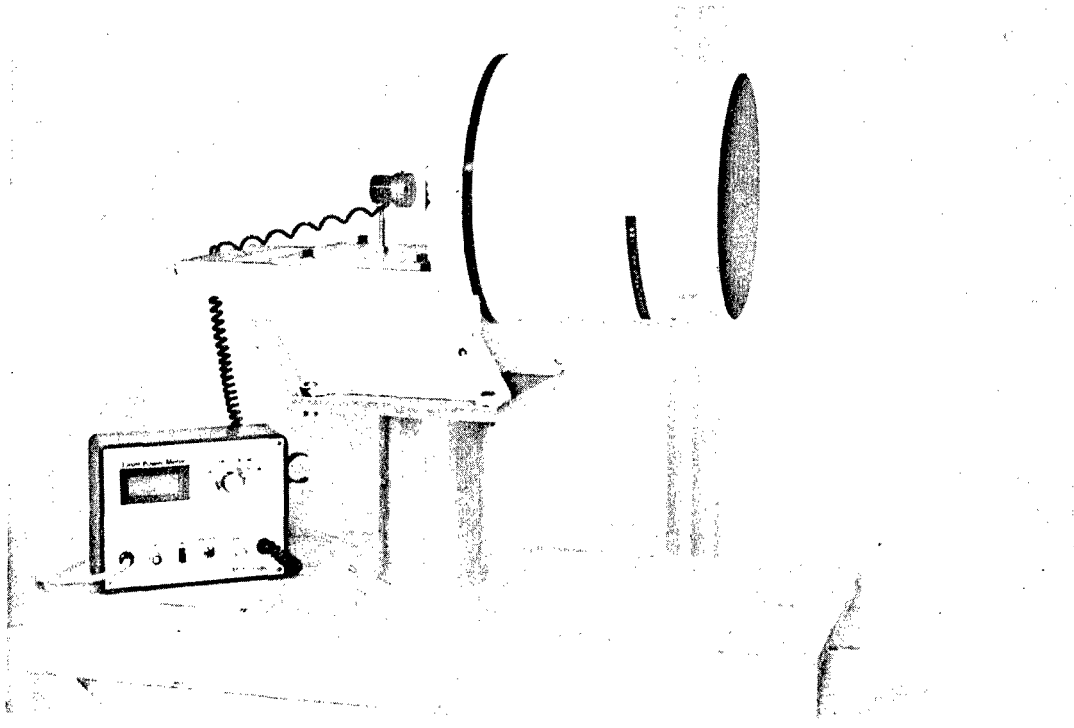

Fig. 14. Laser Receiver

Engineering Transmissometer System, Model 14-708, which consists of a source unit, a receiving unit, and a data logger. The source is a temperature controlled black body with chopper and optics, the receiver consists of a 4-inch diameter germanium lens focussing the radiation on a detector, in front of which is one of four infrared filters mounted on a wheel, and the data logger, containing a phase-locked amplifier, provides both digital and analog measures of percent transmission over a one-kilometer path. The source and receiver are shown in Figures 15 and 16, respectively. The Barnes Transmissometer has been modified to change channels under computer control. This enables data collection in both the 3 to 5 and 8 to 12 micrometer bands almost simultaneously.

The mirror which is located 500 meters from the building is 20 cm in diameter, optically flat, and is coated with aluminum plus a protective overcoat. It is in an adjustable mount on top of a steel column anchored in concrete. The mirror is sheltered from weather by a tubular shroud, which is mounted independently of the mirror support column. The sources and receivers are also sheltered from weather, by an extension of the building.

Transmission data is recorded both on strip charts and digitally. The digitizer is controlled by a microcomputer, which also processes the data. Outdoor transmission measurements are modulated by refractive scintillation, which depends on weather conditions in a complicated way. To arrive at a value of transmission typifying a given time interval, the signal is digitized many times, and the individual samples are averaged to obtain the mean value. To record a measure of the size of refractive scintillations, the standard deviation of the samples is also calculated and recorded. Data are then stored on a floppy disk, and can be examined later on a video display, in a transmission-versus - time format which simulates a strip chart. Interesting time intervals are then further analyzed and plotted on a digital plotter.

The presence of particles in the atmosphere can degrade the performance of imaging systems in more ways than just by lowering transmission: particles can cause a loss of angular resolution by small - angle scattering of radiation from the target into the imaging system, they can reduce thermal contrast by scattering radiation from other

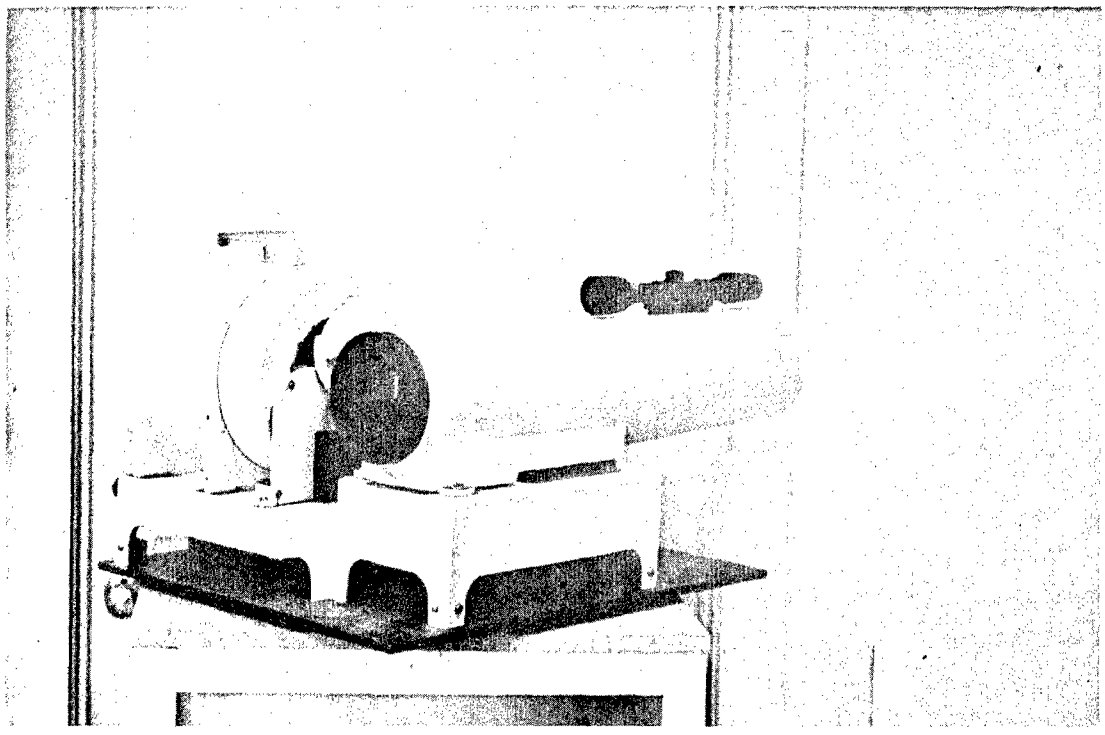

Fig. 15. Barnes Transmissometer Source

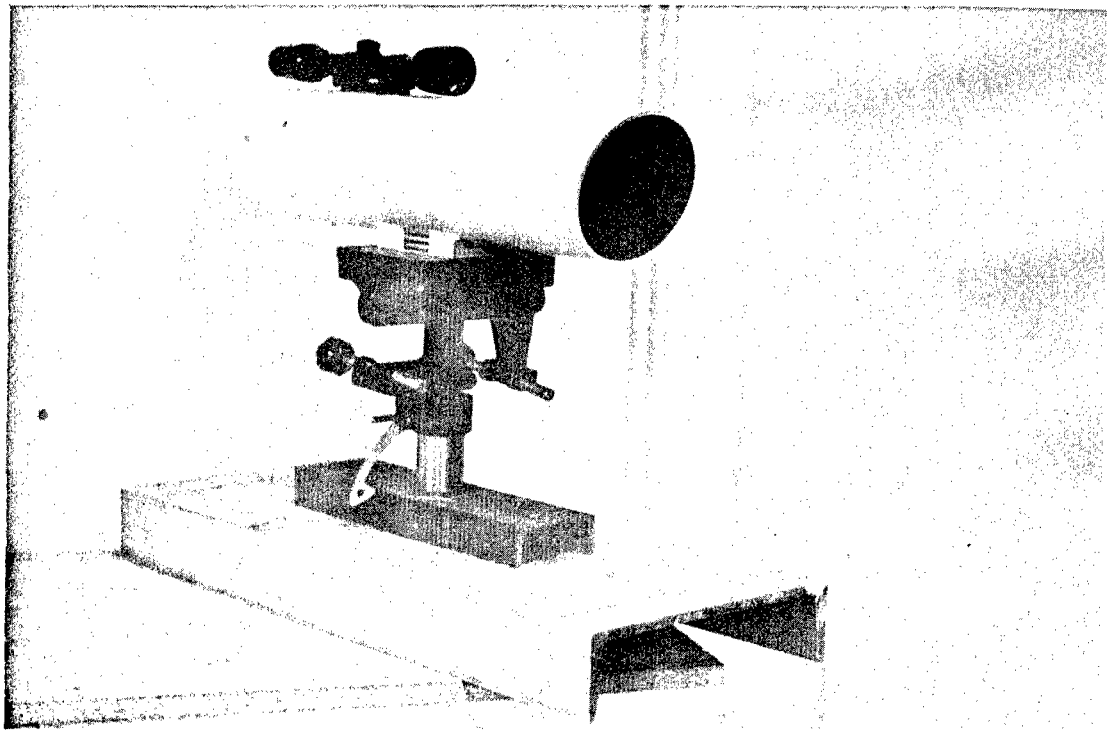

Fig. 16. Barnes Transmissometer Receiver

sources in the imaging system, and in addition, the particles themselves will radiate infrared energy. To study the degradation of imaging system performance in fog, rain, and snow, a portable resolution bar target has been constructed (Figure 17). It consists of a uniformly heated surface with an ambient temperature mask in front of it. The target is heated by passing current through a large sheet of electrically conducting material. The electric power is supplied by a battery, and the target is mounted on a snow vehicle, for portability. The bar target is viewed by two infrared cameras, one operating in the 3 to 5 micrometer range and the other in the 8 to 12 micrometer range. The specifications of these cameras are given in Table 1.

Weather data are necessary to characterize the path during field experiments. For this purpose, a weather station (shown in Figure 18) has been established at KRC, which automatically records the parameters listed in Table 2, in a digital format, at preset time intervals. Besides the standard weather variables, it will be necessary to characterize falling snow for future experiments. This task will be accomplished in two ways: by the use of replicas, and by photographing crystals caught in black trays. Snow crystals will be divided into six main categories (needles, plane dendritic, spatial dendritic, graupel, powder snow, and crystals with droplets) and a given snowfall will be characterized by the size statistics of each category.

Calibration of the transmission range proceeds as follows: the Barnes Transmissometer is calibrated according to the procedure specified by the manufacturer. This basically involves aiming the source and receiver at each other at short range, and placing a small aperture over the black body source. The aperture is of the appropriate diameter to just compensate for the fact that the rays from the source have not diverged before reaching the receiver, as they will when source and receiver are one kilometer apart. The output of the transmissometer is calibrated by noting its output in very clear conditions. This value is taken as being 87 percent transmission, using a β for clear air at 0.63 micrometer of 1.37×10^{-4} m^{-1} (Wolfe and Zissis, 1978). All subsequent output readings are then linearly scaled, using this value.

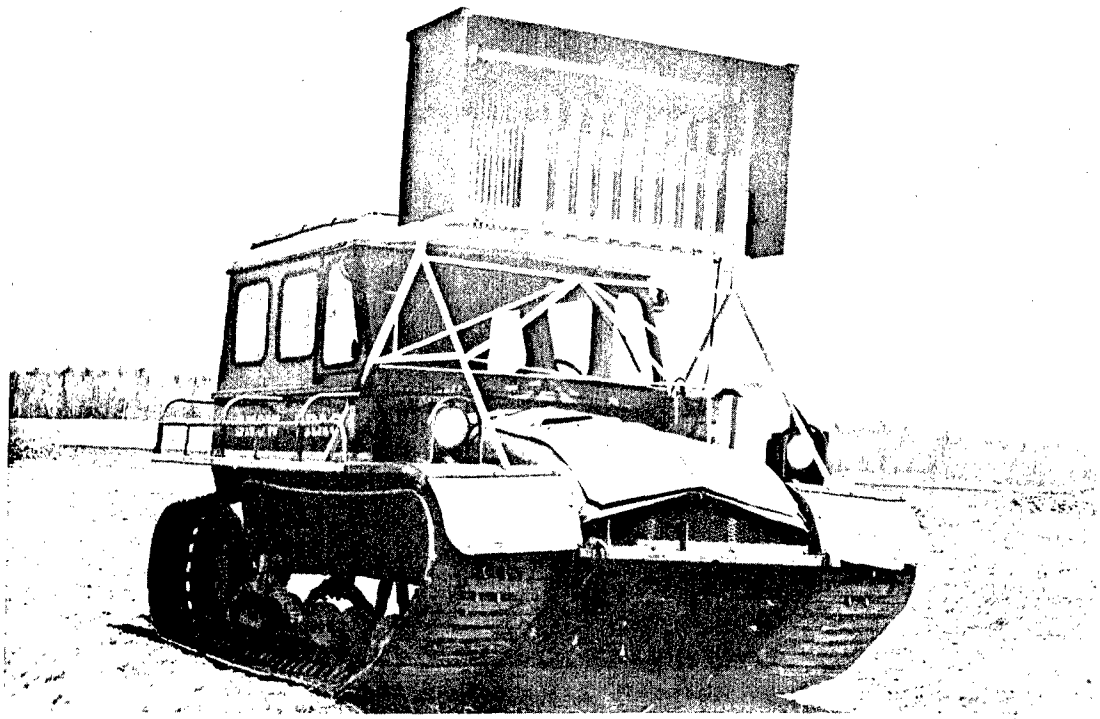

Fig. 17. Resolution Bar Target

Table 1. Infrared Cameras

Make and Model	AGA 661	Bofors T-101
FOV	5°	25°
IFOV	1 mr	5 mr
Frame Rate	16/sec	2/sec
Focus Range	2 m → ∞	0.2 m → ∞
Thermal Resolution	0.2°C at 30°C	0.2°C at 30°C
Temperature Ranges	1, 2, 5, 10, 20, 50, 100, 500, 1000°C	5, 10, 20, 50, 75, 150°C
Thermal Bands	1 to 30% of Temperature Range	2.5 to 20% of Temperature Range
Detector	InSb	HgCdTe
Detector Cooling	LN_2	LN_2

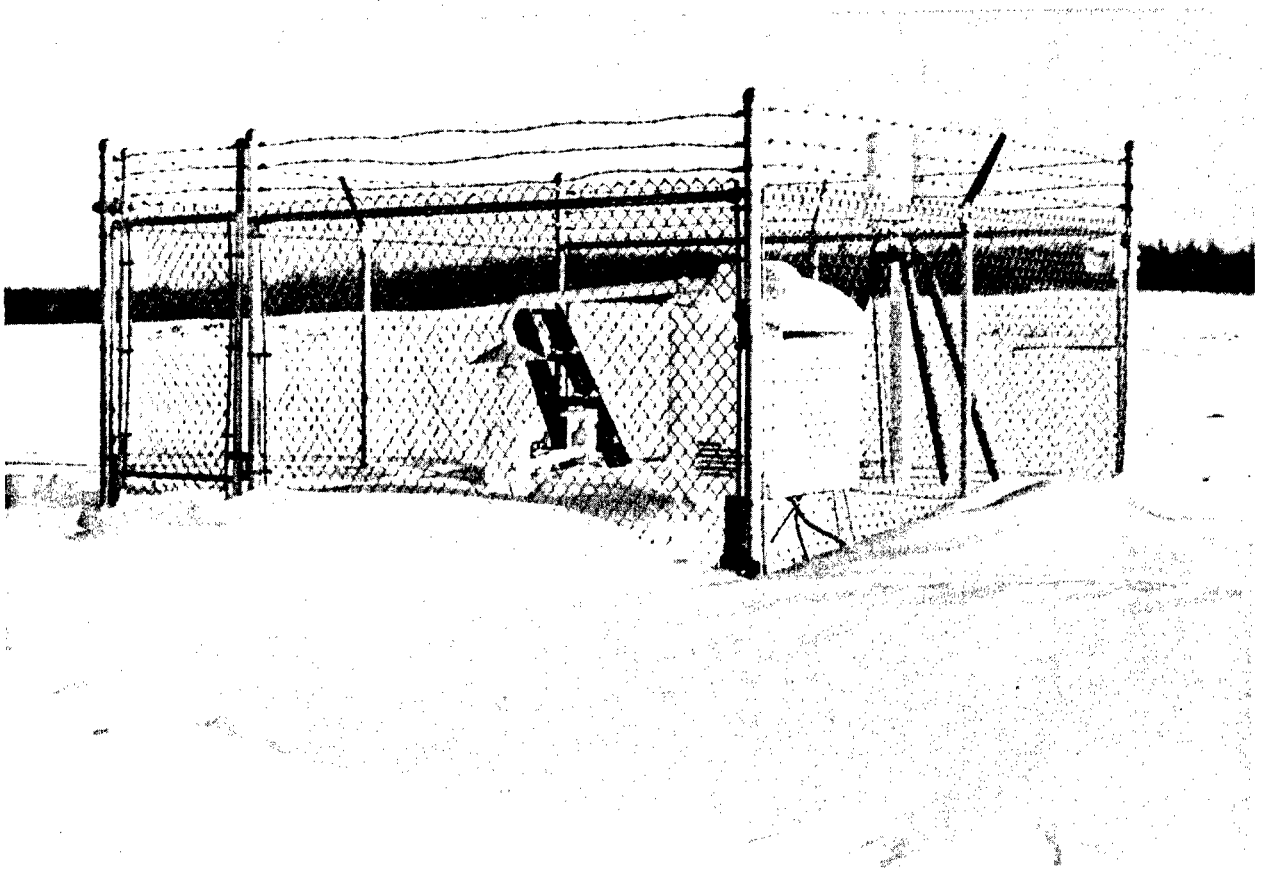

Fig. 18. Weather Station

Table 2. KRC Weather Station

WEATHER PARAMETER	MEASURING INSTRUMENT
Air Temperature	Thermocouple
Ground Temperature	Thermocouple
Asphalt Temperature	Thermocouple
Wind Direction	Wind Vane
Wind Speed	3-Cup Anemometer
Solar Load	Radiometer
Net Solar Load	Net Radiometer
Rainfall/Snowfall	Tipping Bucket
Fog	Visiometer
Smoke & Dust	Nephelometer
Air Pressure	Analog Output Barometer
H_2O Vapor Density	Optical Dewpointer

7. RESULTS

Equations (9) and (11) have shown the importance of the phase function on scattering calculations. If there is little or no scattering, then the scattered intensity terms and hence the phase function is of little importance. The true value of the phase function can be seen in a scattering atmosphere such as a 2-in/hr (50.8 mm/hr) rain. To calculate the phase function and absorption and scattering cross sections for a 50.8 mm/hr rain, the size distribution and the fall velocity of the drops must be considered. The drop distribution of Laws and Parsons (1943) gives the size distribution of drops at any one level per unit time. Using the fall velocity data of Laws (1941), it is possible to calculate the drop size distribution and the cross section of a rain of known intensity in a volume of the atmosphere. The drop size distributions at the surface and in an atmospheric volume (a distance sufficiently below the clouds such that all drops are falling with zero acceleration) are shown in Table 3. The drop distribution in the atmosphere contains a higher percentage of small drops because of slower fall velocities of small drops compared to large drops. The scattering cross section of a 50.8 mm/hr rain is found to be $1.55 \times 10^{-3} m^2$. The phase function is plotted in Figure 19 where a very narrow back scattering peak is observed along with a rainbow around 140°.

To illustrate the importance of the phase function, the transmission of 0.6328 micrometer radiation was calculated using several phase functions in Eqs. (7), (9), and (11). The apparatus parameters were chosen to be those of the KRC Helium-Neon laser transmissometer (receiver optics diameter = 20 cm; receiver angle of acceptance = 11 milliradians). In all cases, the scattering and extinction cross sections of rain were calculated using Mie theory. The average value of $\cos\Theta$ needed for the Henyey-Greenstein phase function $f_{HG}(\Theta)$ was obtained by averaging $\cos\Theta$ over the Mie scattering phase function, which yielded a value of 0.88 corresponding to an angle of 20°. The ratio of forward scattering (0°) to back scattering (180°) of the Mie phase function (2.73×10^7) was used as the parameter s in the Kagiwada - Kalaba phase function $f_{KK}(\Theta)$. A phase function obtained for hexagonal plates of ice by Jacobowitz (1971) using ray tracing was also used, as was a set of experimental data obtained by Huffman and Thursby (1969).

Table III. Size Distribution of Raindrops For a 50.8 mm/hr Rain

Radius (micrometers)	Fraction at Surface	Fraction in Atmosphere
$.625 \times 10^{2}$	.000	.000
$.125 \times 10^{3}$	.000	.000
$.188 \times 10^{3}$	$.100 \times 10^{-2}$	$.264 \times 10^{-2}$
$.250 \times 10^{3}$	$.300 \times 10^{-2}$	$.710 \times 10^{-2}$
$.313 \times 10^{3}$	$.500 \times 10^{-2}$	$.107 \times 10^{-1}$
$.375 \times 10^{3}$	$.700 \times 10^{-2}$	$.133 \times 10^{-1}$
$.438 \times 10^{3}$	$.100 \times 10^{-1}$	$.176 \times 10^{-1}$
$.500 \times 10^{3}$	$.140 \times 10^{-1}$	$.229 \times 10^{-1}$
$.563 \times 10^{3}$	$.170 \times 10^{-1}$	$.259 \times 10^{-1}$
$.625 \times 10^{3}$	$.220 \times 10^{-1}$	$.314 \times 10^{-1}$
$.688 \times 10^{3}$	$.270 \times 10^{-1}$	$.363 \times 10^{-1}$
$.750 \times 10^{3}$	$.310 \times 10^{-1}$	$.387 \times 10^{-1}$
$.813 \times 10^{3}$	$.360 \times 10^{-1}$	$.433 \times 10^{-1}$
$.875 \times 10^{3}$	$.410 \times 10^{-1}$	$.469 \times 10^{-1}$
$.438 \times 10^{3}$	$.460 \times 10^{-1}$	$.509 \times 10^{-1}$
$.100 \times 10^{4}$	$.760 \times 10^{-1}$	$.802 \times 10^{-1}$
$.112 \times 10^{4}$	.106	.104
$.125 \times 10^{4}$	.104	$.964 \times 10^{-1}$
$.137 \times 10^{4}$	$.936 \times 10^{-1}$	$.818 \times 10^{-1}$
$.150 \times 10^{4}$	$.780 \times 10^{-1}$	$.661 \times 10^{-1}$
$.162 \times 10^{4}$	$.670 \times 10^{-1}$	$.554 \times 10^{-1}$
$.175 \times 10^{4}$	$.550 \times 10^{-1}$	$.444 \times 10^{-1}$
$.188 \times 10^{4}$	$.430 \times 10^{-1}$	$.339 \times 10^{-1}$
$.200 \times 10^{4}$	$.340 \times 10^{-1}$	$.265 \times 10^{-1}$
$.212 \times 10^{4}$	$.240 \times 10^{-1}$	$.183 \times 10^{-1}$
$.225 \times 10^{4}$	$.170 \times 10^{-1}$	$.128 \times 10^{-1}$
$.237 \times 10^{4}$	$.120 \times 10^{-1}$	$.895 \times 10^{-2}$
$.250 \times 10^{4}$	$.900 \times 10^{-2}$	$.671 \times 10^{-2}$
$.262 \times 10^{4}$	$.700 \times 10^{-2}$	$.516 \times 10^{-2}$
$.275 \times 10^{4}$	$.500 \times 10^{-2}$	$.369 \times 10^{-2}$
$.287 \times 10^{4}$	$.400 \times 10^{-2}$	$.295 \times 10^{-2}$
$.300 \times 10^{4}$	$.300 \times 10^{-2}$	$.221 \times 10^{-2}$
$.313 \times 10^{4}$	$.200 \times 10^{-2}$	$.148 \times 10^{-2}$
$.325 \times 10^{4}$	$.200 \times 10^{-2}$	$.148 \times 10^{-2}$

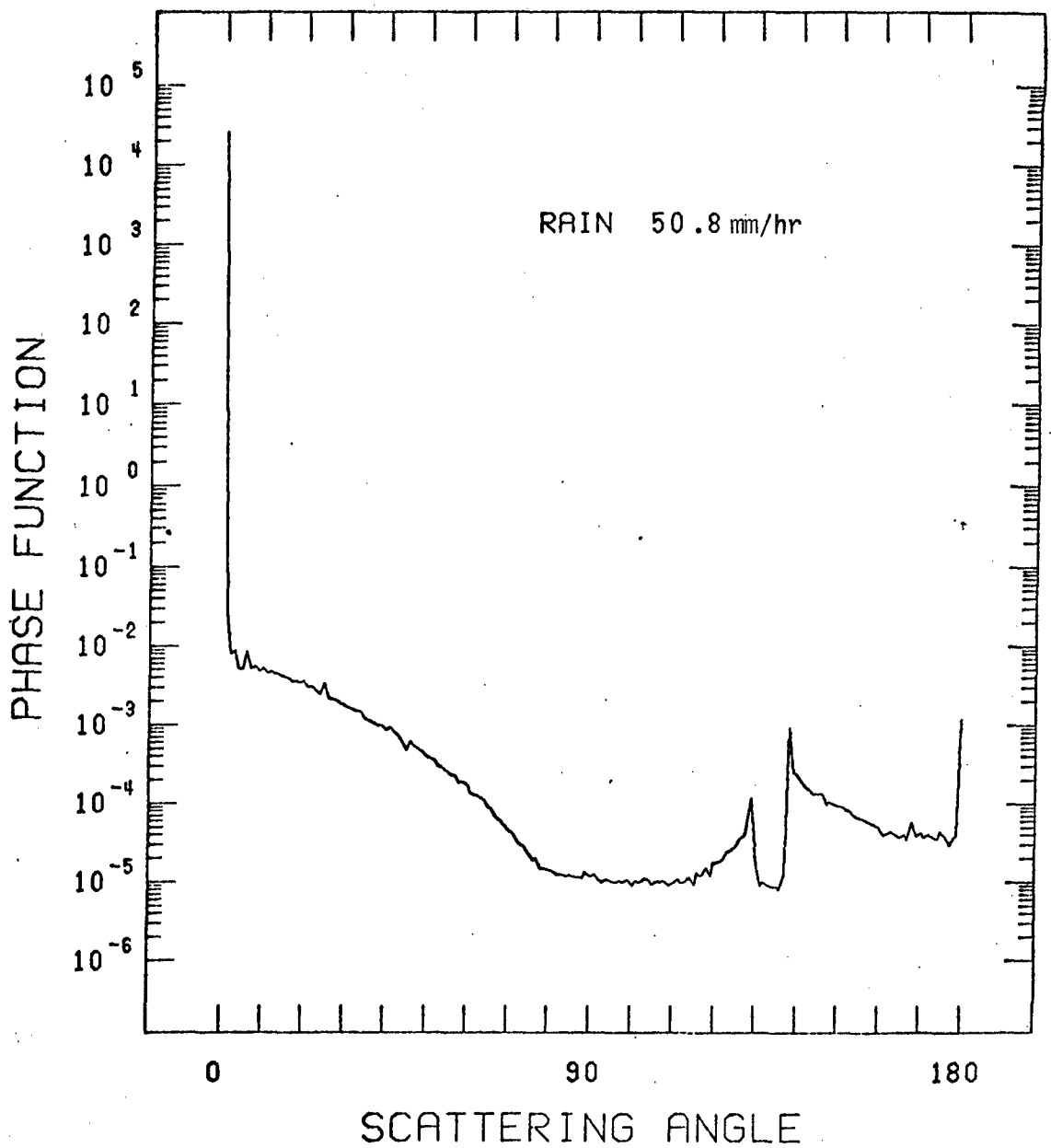

Fig. 19. Phase function of a 50.8 millimeter/hour rain calculated using Mie theory for the rain drop distribution of Laws and Parsons.

The data of Huffman and Thursby was extrapolated to 0° and 180° to cover regions inaccessible by experimental means. The Rayleigh and isotropic phase functions were also used in the computation, even though they describe scattering by small particles. All sizes of the rain drops considered are large compared with the wavelength of visible light and therefore strong forward scattering is expected. The results of the comparison are shown in Table 4. As expected, the Rayleigh and isotropic phase functions do not predict that as much scattered intensity will reach the detector as does the Mie phase function. The same result occurs for both the Jacobowitz, and modified Huffman-Thursby phase function. The modified phase function could be corrected by increasing the extrapolated height of the forward scattering peak. The analytic phase functions also predict intensities differing from that predicted using Mie theory.

When comparing the attentuation of two or more different wavelengths, it is important to examine and understand the limitation placed on the measurements by the experimental apparatus. Before attempting to attribute attenuation to scattering, it must be ascertained how receptive the apparatus is to scattered light. Using a 1.26 mm/hr rain as a scattering medium, the effect of receiver field of view is shown in Figure 20 for a large transmissometer with a 0.5 cm detector viewing a 1-watt laser at 1 kilometer. Since the laser is assumed to be nondivergent, the received power due to first order scattering depends only on the size of the receiver and not the field of view. The power received after experiencing two scattering events increases rapidly with increasing field of view before leveling off. Such calculations are also dependent on phase function. The effect of receiver size is shown in Figure 21 where both first and second order scattering contribution to received power increase with increasing receiver size. Here a laser transmissometer with a 5 milliradian field of view viewing a 1-watt laser at 1 kilometer was assumed. For a half meter detector, the received power which has undergone exactly one scattering event amounts to 60 milliwatts. In such a case, attributing the total received power to radiation which has not experienced a scattering or absorption process (as is done in the GAP model) would lead to a substantial error in the extinction coefficient.

Table IV. Scattering Contribution to Received Power for Transmission in a 50.8 mm/hr Rain

	Unscattered	First Order S	Second Order D	Total
Mie Polydispersion	.185	$.395 \times 10^{-1}$	$.433 \times 10^{-4}$	.225
Henyey-Greenstein	.185	$.567 \times 10^{-3}$	$.196 \times 10^{-5}$	.186
Kagiwada-Kalaba	.185	.262	$.261 \times 10^{-3}$	.447
Jacobowitz	.185	$.178 \times 10^{-2}$	$.263 \times 10^{-5}$	.187
Huffman-Thursby	.185	$.303 \times 10^{-4}$	$.369 \times 10^{-7}$	.185
Rayleigh	.185	$.261 \times 10^{-5}$	$.105 \times 10^{-7}$	.185
Isotropic	.185	$.138 \times 10^{-6}$	$.757 \times 10^{-10}$	.185

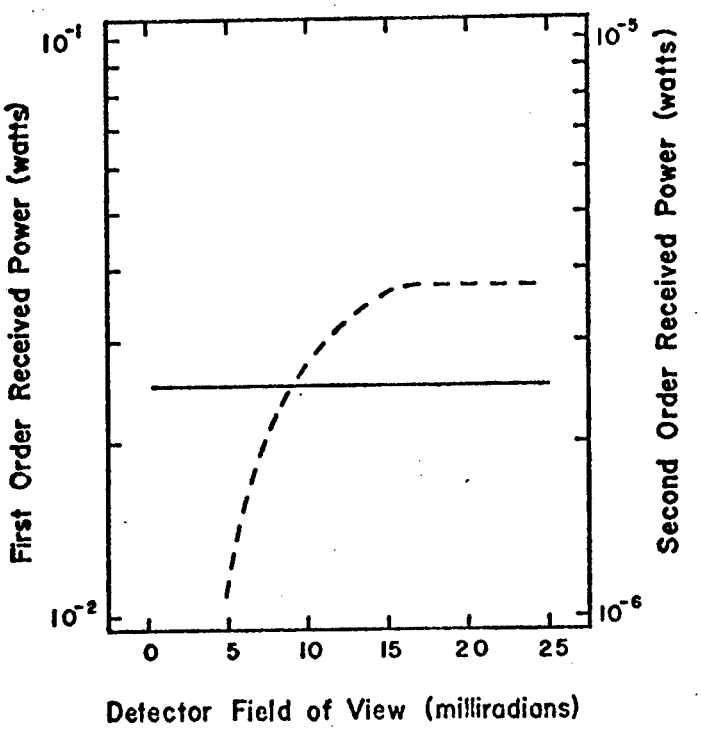

Fig. 20. Effect of detector field of view on received power. Power received after first order scattering (——) does not depend on the receiver field of veiw because the laser is assumed to be non-divergent. Second order received power (----) increases until a constant level is observed at about 15 milliradions. The scattering medium was assumed to be a 1.26 mm/hr rain.

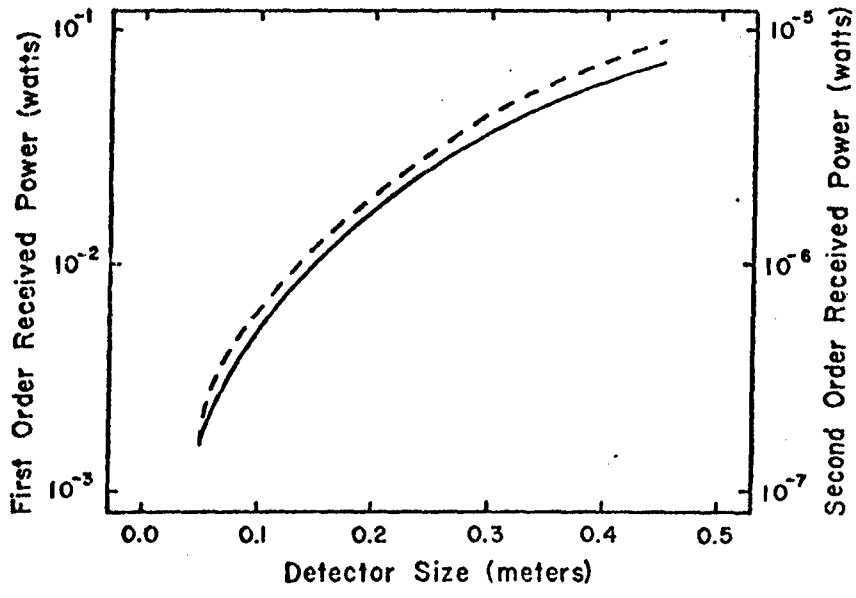

Fig. 21. Effect of detector size on received power. Both first order (——) and second order (----) contributions increase with increasing detector size. The scattering medium was assumed to be a 1.26 mm/hr rain.

Using the three rainfall rates of 0.25, 1.26, and 6.60 mm/hr, the attenuation coefficients at 0.6328 and 10.59 micrometers may be compared for the experimental apparatus used in the optics laboratory at the Keweenaw Research Center (Figure 22). Note that the calculation which ignores scattering agrees fairly well with the GAP model. When first and second order scattering is included it departs from the GAP model. This is due to scattering being more prevalent for 0.6328 micrometer than 10.59 micrometers and the larger field of view and receiver size of the 0.6328 micrometer laser transmissometer. A similar comparison is shown in Figure 23 between 3.65 and 0.6328 micrometer radiation. The poor agreement is due to the GAP model being a band average over the 3 to 5 micrometer band while the calculation was done for a very narrow laser line.

The results reported here are from measurements in which infrared and visible transmissions were measured simultaneously, but rainfall/snowfall rates were not recorded. The extinction coefficients from the measured transmission values can be presented conveniently by plotting the logarithms of the infrared extinction coefficients versus the logarithms of the visible extinction coefficients. Early results for snow are shown in this format in Figure 24. Also shown is the prediction for the GAP model, which fits the data fairly well. A similar measurement was recently reported by a Swedish group (Eklund, et al., 1978) who used a 10.6 micrometer laser and a 0.6328 micrometer laser to measure transmissions in falling snow. They reported their results as decibels of attenuations versus time; the analysis of their data in the format mentioned above is shown in Figure 25. The Swedish results can be seen to lie close to the GAP model, except for seven points for which the infrared extinction is anomalously high. These seven points occurred sequentially in time, in weather documented only as heavy snow. The explanation for this is not known, but this result serves to show the utility of the log-log format, in which such anomalies are readily apparent.

Measurements at KRC in the 8 to 12 micrometer band in rain and fog are shown in Figure 26, along with the GAP model predictions. The agreement in rain is fair, but in fog, larger infrared extinctions

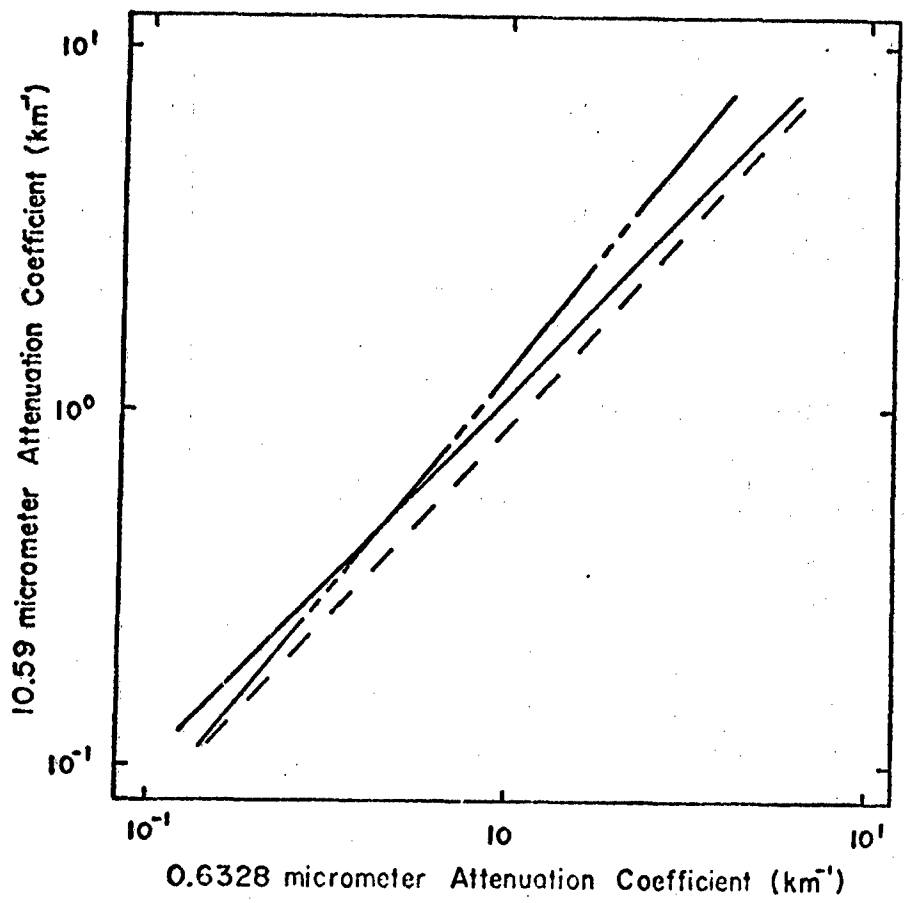

Fig. 22. Comparison of attenuation at 10.59 and 0.6328 micrometers by a monodisperse rain. Calculations with (——--——) and without (----) scattering contributions are compared with the GAP model (——).

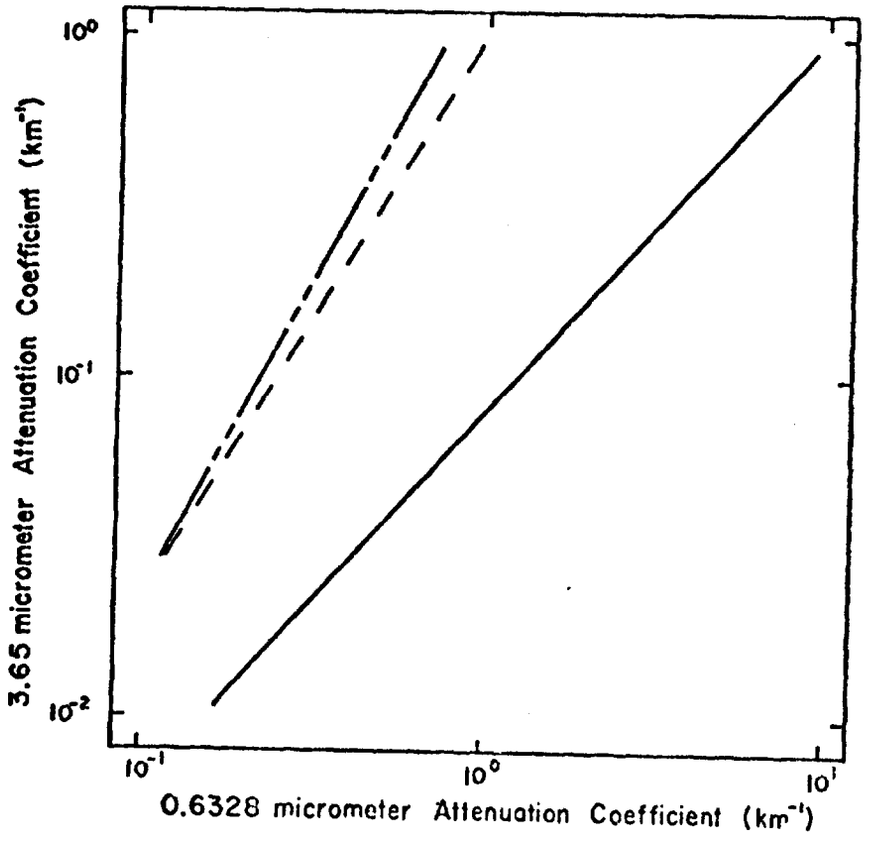

Fig. 23. Comparison of attenuation at 3.65 and 0.6328 micrometers by a monodisperse rain. Calculation with (——-——) and without (----). Scattering contributions are compared with the GAP model (-). The GAP model is band averaged over the 3 to 5 micrometer band while the computation assumed a very narrow Laser line.

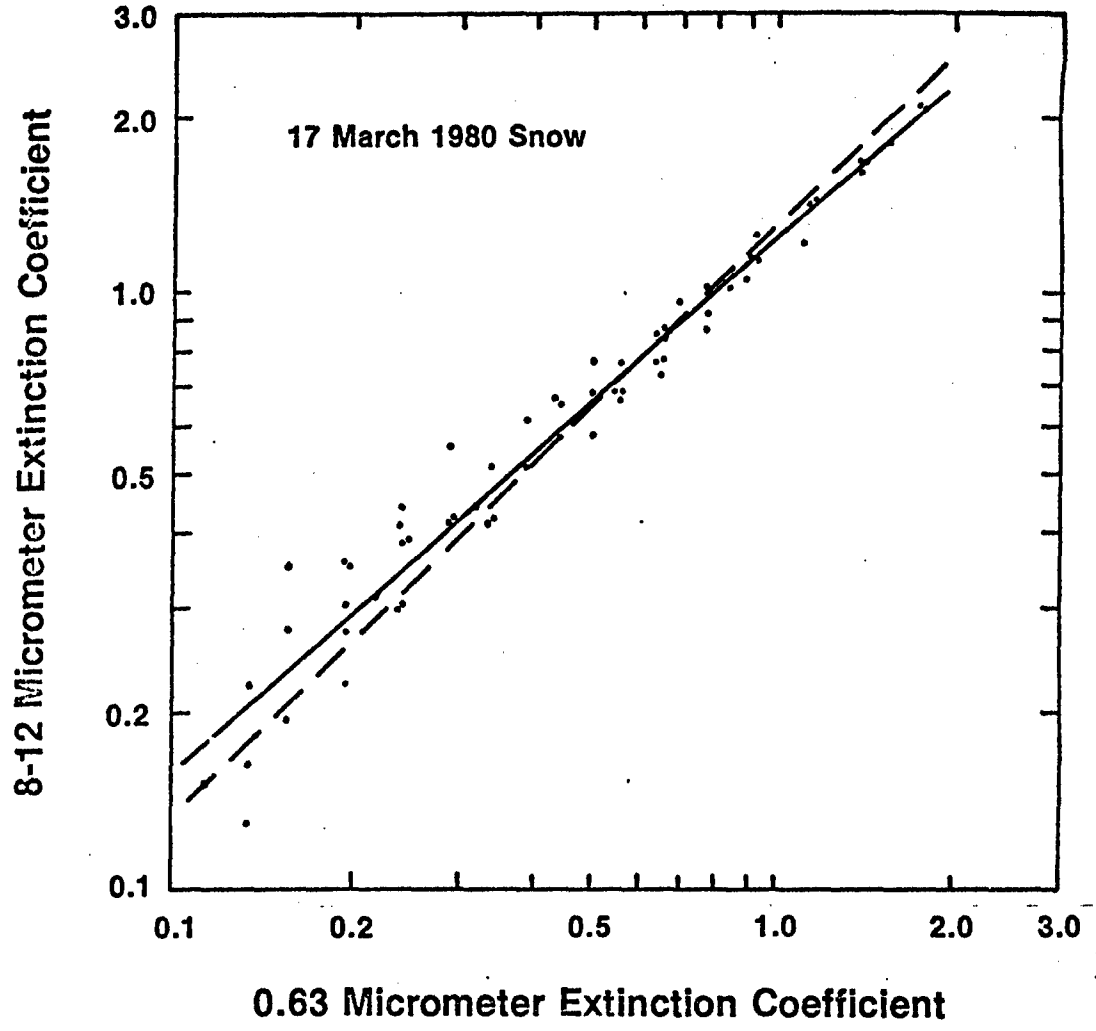

Fig. 24. Snow data recorded at KRC. The solid line was fitted to the data by the method of least squares; the dashed line is the GAP model.

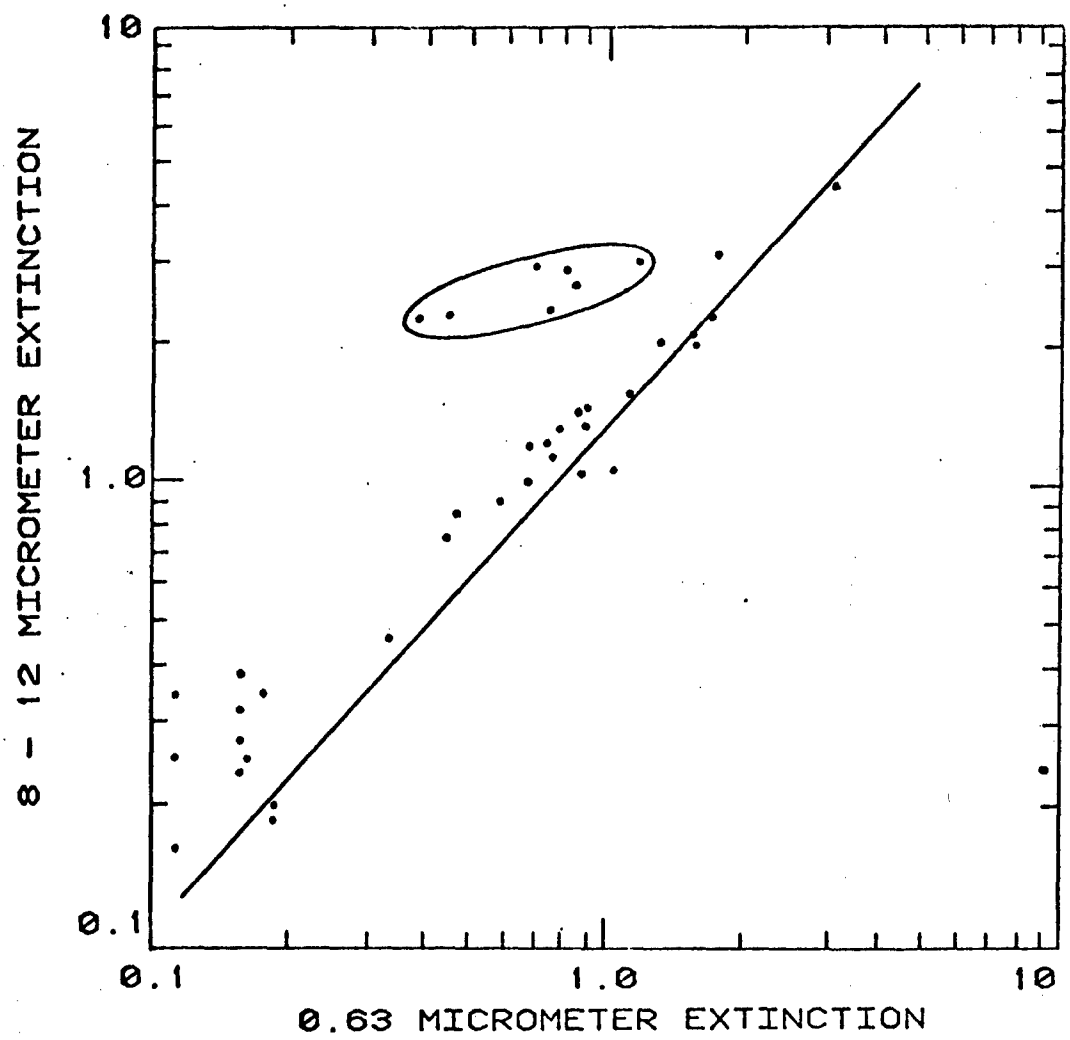

Fig. 25. Snow data recorded in Sweden by Eklund, et.al. (1978).

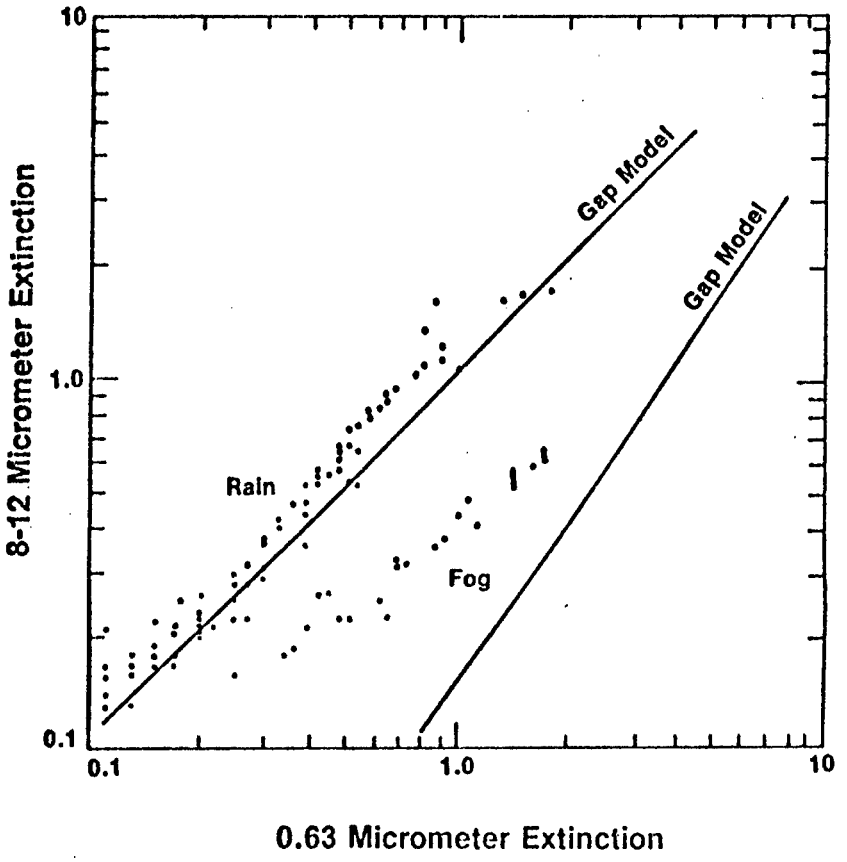

Fig. 26. Rain and fog data recorded at KRC. The rain data lies close to the GAP prediction, but measured fog extinctions are considerably higher than the model predicts.

are observed than the model predicts. This was generally true in fog measurements, in both the 8 to 12 micrometer range and the 3 to 5 range, as shown in Figure 27.

The fog data shown here tend to be better behaved (in terms of a correlation between infrared and visible extinction coefficients) than other published fog results (such as the A.P. Hill data shown by Turner, et al., 1980). The reason for this becomes apparent when one considers the time variable. The atmosphere at one instant of time will have one value of infrared extinction coefficient and one value of visible extinction coefficient, and of course will correspond to one point on the log - log graph of these two quantities. As the atmosphere changes in time, it does so continuously, so that point on the graph moves continuously. If one follows the formation or dissipation of a fog by making measurements at short enough time intervals so as to have many measurements during the course of the fog evolution, one gets data points lying along a straight line in the log-log format. A striking example of this is shown in Figure 28, where a fog is observed in the processes of forming, dissipating, and reforming. The lines which represent these three processes depend on meteorological processes in a way which remains to be investigated, but it is apparent that the large scatter of fog data points in other measurements is caused by sampling at time intervals large compared to the characteristic time of fog evolution, and the good correlations observed between the two extinction coefficients at KRC suggest that a better model can be formulated, if evolution in time is considered.

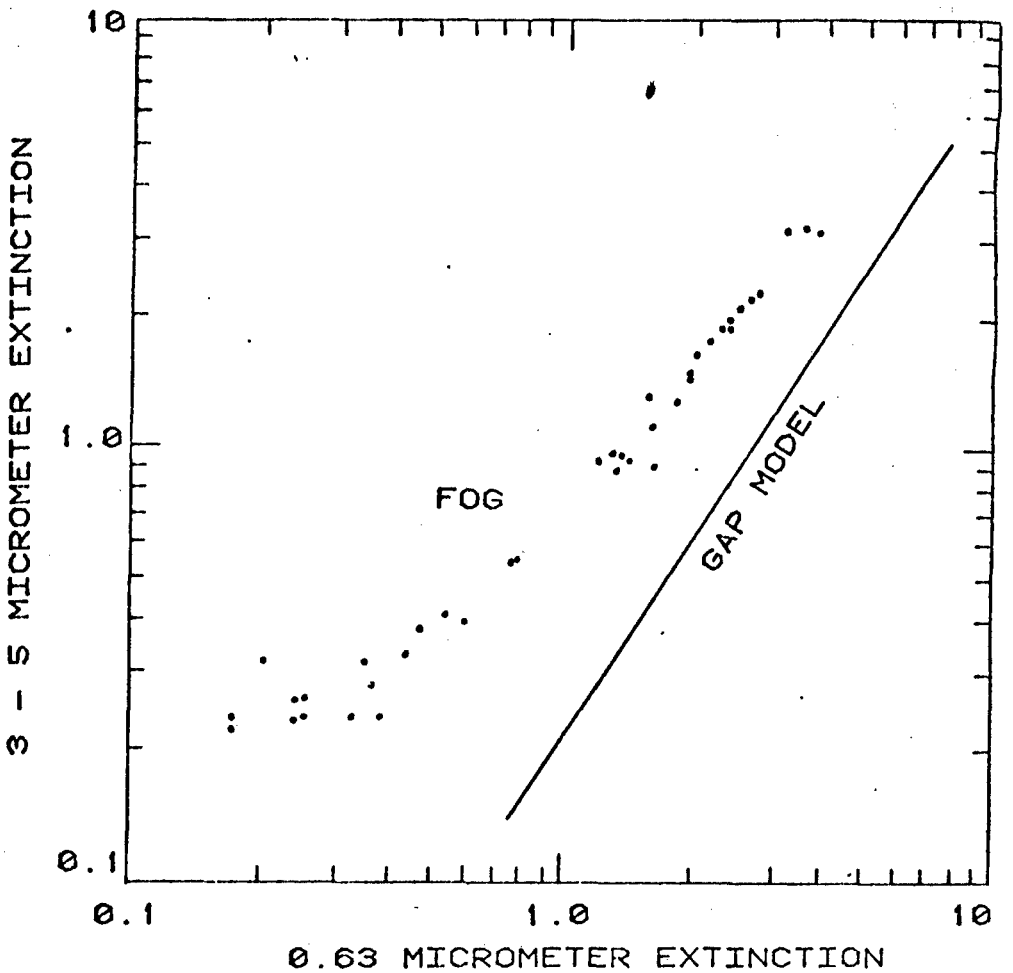

Fig. 27. Fog data recorded at KRC. In the 3-5 micrometer range, measured fog extinctions tend to be higher than GAP model predictions.

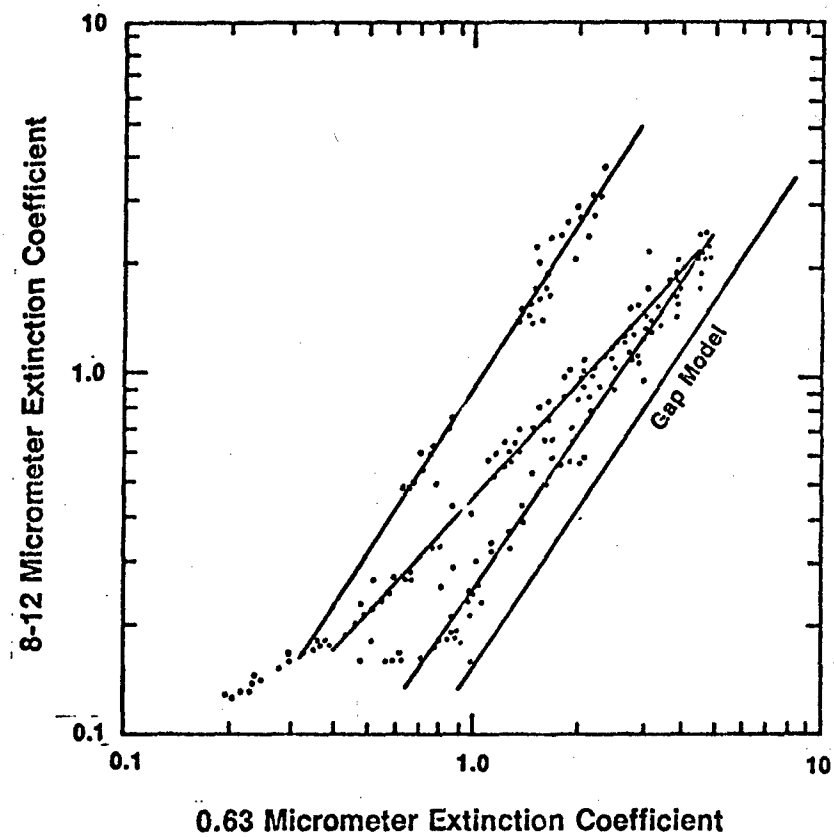

Fig. 28. History of fog extinctions. The fog formed (line closest to GAP model), dispersed, and formed again, following paths given roughly by the straight lines, which have been sketched in to guide the eye.

REFERENCES

Barteneva, O.D., Dougyallo, Ye.N., and Polyakova, Ye.A., Tr. GGO (1967).

Bisyarin, V.P., Bisyarina, I.P., Ruback, V.K., and Sokolov, A.V., Radio Eng. Electron. Phys. 16 1594-1597 (1971).

Best, A.C., Quart. J. Ray. Meteorol. Soc. 76 16-36 (1950).

Bruscaglioni, P., Optics Commun. 27 9-12 (1978).

Bruscaglioni, P., Lett. Nuovo Cimento 24 485-488 (1979).

Bruscaglioni, P. and Ismaelli, A., Nuovo Cimento 1C 147-166 (1978).

Bruscaglioni, P. and Ismaelli, A., Optica Acta 26 679-691 (1979).

Chu, T.S. and Hogg, D.C., B.S.T.J. 47 723-759 (1968).

Duncan, L.D., Shirkey, R.C., Sutherland, R.A., Avara, E.P., and Monahan, H.H., ASL-TR-0047 (1979).

Eklund, H., Lundqvist, S., Marthinsson, B., and Eng, S.T., Infrared Physics 18 337-342 (1978).

Fabelinskii, I.L., Molecular Scattering of Light, Plenum Press, New York, 1968.

Henyey, L.G. and Greenstein, J.L., Astrophysics J. 93 70-83 (1941).

Huffman, P.J. and Thursby, W.R., J. Atmos. Sci. 26 1073-1077 (1969).

Jacobowitz, H., J. Quant. Spectrosc. Radiat. Transfer 11 691-695 (1971).

Jessen, W., Kohnle, A., Hipp, H., and Hohn, D.H., Infrared Phys. 20 175-183 (1980).

Kagiwada, H. and Kalaba, R., Rand Report RM-5537-PR, Rand Corporation, Santa Monica, CA, 1967.

Kerker, M., The Scattering of Light, Academic Press, New York, 1969.

Laws, J.O., Trans. Am. Geophys. 22 709-721 (1941).

Laws, J.O. and Parsons, D.A., Trans. Am. Geophys. 24 452-460 (1943).

McClatchey, R.A., Benedict, W.S., Clough, S.A., Burch, D.D., Calfee, R.F., Fox, K., Rothman, L.S., and Goring, J.S., AFCRL-TR-73-0096 (1973).

Mie, G., Ann. Physik 25 377-445 (1908).

Moulton, J.R., Bergeman, R.J., and Sola, M.C., IRIS Symposium, 1976.

Rensch, D.B. and Long, R.K., Appl. Optics 9 1563-1573 (1970).

Selby, J.E.A., Kneizys, F.X., Chetwynd, Jr., J.H., and McClatchey, R.A., AFGL-TR-78-0053 (1978).

Shields, F.S., NV&EOL Internal. Memorandum, 1978.

Shifrin, K.S., Scattering of Light in a Turbid Medium, NASA TT F-477 (1968).

Smith, H.J.P., Duke, D.J., Gardner, M.E., Clough, S.A., Kneizys, F.X. and Rothman, L.S., AFGL-TR-78-0081 (1978).

Sokolov, A.V. and Sukhonin, Ye.V., Radio Eng. Electron. Phys. 15 2167-2171 (1971).

Turner, R.E., Gebhardt, F.G., Manning, J.L., Meredith, R.E., Singer, S.M., Smith, F.G., and Vavra, P.C., ASL-CR-80-0177 (1980).

Van de Hulst, H.C., Light Scattering by Small Particles, Wiley, New York, 1957.

Winchester, Jr., L.W., Choi, W.K., Gimmestad, G.G., Lee, S.M., and Parks, P.N., Proc. 2nd KRC Symp. on Ground Vehicle IR Signature 1 123-131 (1980a)

Winchester, Jr., L.W., Choi, W.K., Gimmestad, G.G., Lee, S.M., and Parks, P.N., JOSA 70 1561 (1980b).

Winchester, Jr. L.W., Gimmestad, G.G., and Wetzel, R.B., Proc. Int. Union of Radio Sci. XXth Assembly (1981).

Wolfe, W.L. and Zissis, G.J., The Infrared Handbook, ONR, Washington, D.C., 1978.

ADDRESSEE	NO. OF COPIES
Commander US ARMY TANK-AUTOMOTIVE COMMAND WARREN, MI 48090	
ATTN: DRCPM-M60	1
DRCPM-GCM	1
DRCPM-FVS	1
DRSTA-TSL	5
DRSTA-ZSC 25	25
Director Defense Advanced Research Projects Agency 1400 Wilson Blvd. Arlington, VA 22314	1
Commander Harry Dimond Laboratories ATTN: DRXBO-RAL Aldelphi, MD 20783	1
Defense Documentation Center Cameron Station Alexandria, VA 22314	15
Commander US Army Missile Research and Development Command ATTN: DRDM1-TEI Redstone Arsenal, AL 66027	2
Director US Army Materiel Systems Analysis Agency ATTN: DRXSY-T Aberdeen Proving Ground, MD 21005	1
Commander US Army Armor and Engieer Board ATTN: ATZK-AE-TE-E Ft. Knox, KY 40121	1
Commander US Army Mobility Equipment R&D Command ATTN: DRDME-RT Ft. Belvoir, VA 22060	2
USA Human Engineering Laboratory Aberdeen Proving Ground, MD 21010	2